4-2003

# Improved Lagrangian mixing models for passive scalars in isotropic turbulence

Rodney O. Fox
*Iowa State University*, rofox@iastate.edu

P. K. Yeung
*Georgia Institute of Technology - Main Campus*

# Improved Lagrangian mixing models for passive scalars in isotropic turbulence

R. O. Fox and P. K. Yeung

Citation: Physics of Fluids (1994-present) **15**, 961 (2003); doi: 10.1063/1.1545472
View online: http://dx.doi.org/10.1063/1.1545472
View Table of Contents: http://scitation.aip.org/content/aip/journal/pof2/15/4?ver=pdfcov
Published by the AIP Publishing

# Improved Lagrangian mixing models for passive scalars in isotropic turbulence

R. O. Fox[a)]
*Department of Chemical Engineering, Iowa State University, Ames, Iowa 50011-2230*

P. K. Yeung
*School of Aerospace Engineering, Georgia Institute of Technology, Atlanta, Georgia 30332-0150*

(Received 21 June 2002; accepted 17 December 2002; published 4 March 2003)

Lagrangian data for velocity, scalars, and energy and scalar dissipation from direct numerical simulations are used to validate Lagrangian mixing models for inert passive scalars in stationary isotropic turbulence. The scalar fluctuations are nearly Gaussian, and, as a result of production by uniform mean gradients, statistically stationary. Comparisons are made for Taylor-scale Reynolds numbers in the range 38 to about 240 and Schmidt numbers in the range 1/8 to 1. Model predictions for one-point, one-time Eulerian statistics (*Eulerian correspondence*) and one-particle, two-time Lagrangian statistics (*Lagrangian correspondence*) are examined. Two scalar mixing models, namely the Lagrangian Fokker–Planck model and the Lagrangian colored-noise (LCN) model, are proposed and written in terms of stochastic differential equations (SDE) with specified drift and diffusion terms. Both of these models rely on statistics of the scalar field conditioned upon the energy dissipation, as provided by the Lagrangian spectral relaxation (LSR) model. With the exception of the scalar dissipation, the models are shown to capture the Reynolds and Schmidt-number dependence of the Lagrangian integral time scales. However, the LCN model provides a more realistic description of the Lagrangian scalar fluctuations as differentiable time series having the correct form of the scalar autocorrelation function. Further extensions of the new mixing models to non-Gaussian scalars are conceptually straightforward, but require a closure for the scalar-conditioned scalar dissipation rate matrix. Likewise, accurate prediction of joint statistics for differential diffusion between different scalars with unequal molecular diffusivities will require the formulation of a multiscale SDE similar to the LSR model. © *2003 American Institute of Physics.* [DOI: 10.1063/1.1545472]

## I. INTRODUCTION

The mixing of passive scalars in turbulent flow is a crucial process in a wide range of industrial applications, including combustion devices where multiple chemical species of different molecular diffusivities are routinely encountered. A modeling approach of increasing utility for this type of problem is the probability density function (PDF) method, which is based on evolution equations for the PDFs of fluctuations of turbulent flow variables. It is well-known[1,2] that both the modeling and the subsequent numerical implementation are most naturally carried out in a Lagrangian framework following the paths of infinitesimal fluid particles, which together constitute the fluid medium. Although PDF methods also have the advantage of nonlinear convective and reaction terms appearing in closed form, major challenges remain in the modeling of molecular mixing in a Lagrangian frame. Pope[2] has noted that, for several reasons, Lagrangian modeling of passive scalars is more difficult than the corresponding task for the velocity field. The difficulties are more pronounced when differential diffusion between multiple scalars must be considered.

For our present purposes the primary objective of Lagrangian mixing models is to describe the Lagrangian time history $\{\phi^+(t)\}$ of scalar fluctuations in a quantitative manner, including the effects of the transporting velocity field (given by the Reynolds number) and finite molecular diffusivity (given by the Schmidt number). Because the scalar fluctuations are advected in space, information on length scale or spatial structure of the scalar fields represented by local scalar gradient fluctuations is important. Furthermore, since scalar mixing depends on how energy, or spectral content, is passed on from the large scales to the small scales, one can expect the rate of energy transfer between the large scales and small scales in the velocity field to be an important parameter. This energy transfer is, of course, well represented by the energy dissipation rate, $\epsilon$. A successful Lagrangian mixing model should thus include appropriate roles for both energy and scalar dissipation rates in the formulation. The Lagrangian spectral relaxation (LSR) model of Fox[3,4] is one that satisfies, at least in principle, these basic requirements.

The LSR model was originally introduced to provide a simple Lagrangian description of Reynolds and Schmidt number effects on the time evolution of a *nonequilibrium* scalar spectrum (e.g., due to initial conditions) towards its

a)Telephone: (515) 294-9104; fax: (515) 294-2689; electronic mail: rofox@iastate.edu

 

fully developed form. In this work, this feature of the model is not required; however, the multiscale description of the scalar spectrum used in the LSR model also allows for the description of scalars with different Schmidt numbers.[4] As shown by Yeung,[5] the correlation between two scalars with different Schmidt numbers depends strongly on scale size as expressed in wavenumber space. In the LSR model, scalar decorrelation is generated in the dissipation range of the scalar spectrum and transported back to larger scales. Because the contributions to the scalar variance from the dissipation range decreases with increasing Reynolds number, the magnitude of scalar decorrelation predicted by the LSR will be smaller at higher Reynolds numbers.[4] In the context of Lagrangian mixing models, the primary role of the LSR model is to supply the dissipation rates for the scalar variances and covariances in the form of the Lagrangian scalar dissipation rate matrix $\chi^*$. In addition to providing the characteristic time scales for scalar mixing, this matrix ultimately determines the degree of correlation between the scalars. For example, for completely uncorrelated scalar fields, $\chi^*$ will be a full-rank, diagonal matrix, while for completely correlated scalars it will be of rank one. The form and rank of $\chi^*$ depend on a number of factors (initial conditions, orientation of mean scalar gradients, Schmidt numbers, etc.) that must be carefully considered when developing a general model.[4] In the present work, we consider only fully developed scalar fields with collinear mean gradients. Thus, the primary role of the LSR model will be to provide a consistent model for $\chi^*$ for two scalars with different Schmidt numbers.

The principal modeling objective in Lagrangian PDF methods is to achieve agreement between the statistics of fluid–particle and notional–particle variables.[2,6] In this work, we shall denote Eulerian fields with no superscript, the corresponding Lagrangian fluid–particle variables with a superscript $^+$, and the Lagrangian notional–particle variables with a superscript *. In a Lagrangian PDF framework, *Eulerian correspondence* requires that the statistics of the notional particles must agree with the one-point, one-time Eulerian field statistics. For example, the notional–particle velocity $u^*(t)$ must satisfy

$$\langle u(\mathbf{x},t)\rangle = \langle u^*(t)|\mathbf{X}^*(t)=\mathbf{x}\rangle = 0 \tag{1}$$

and

$$\langle u(\mathbf{x},t)u(\mathbf{x},t)\rangle = \langle u^*(t)u^*(t)|\mathbf{X}^*(t)=\mathbf{x}\rangle, \tag{2}$$

where $\langle \cdot|\mathbf{X}^*(t)=\mathbf{x}\rangle$ is the expected value conditioned on the notional–particle location.[6] In addition, *Lagrangian correspondence* requires agreement at the level of one-particle, multitime statistics. For example, two-time Lagrangian correspondence between $u^+(t)$ and $u^*(t)$ is achieved when

$$\langle u^+(t)u^+(t+\tau)\rangle = \langle u^*(t)u^*(t+\tau)\rangle. \tag{3}$$

Thus, one key objective of this work is to develop a Lagrangian mixing model that achieves both Eulerian and two-time Lagrangian correspondence for all modeled quantities (i.e., velocity, turbulent dissipation rate, scalars, and scalar dissipation rates) over a wide range of Reynolds and Schmidt numbers.

One long-standing difficulty in the development of Lagrangian stochastic models is the general scarcity of data suitable for model testing. Lagrangian measurements in the laboratory are extremely difficult; despite recent progress in measurements of velocity and acceleration,[7–9] no such data for scalars from experiments are known. However, recently[10] Lagrangian statistics of scalars have been obtained from direct numerical simulations (DNS), for the base case of isotropic turbulence with stationarity maintained in both the velocity and scalar fields. Despite limitations in the Reynolds number, DNS has a clear advantage in the degree of detail available.

The best use of DNS for stochastic modeling involves two key steps. The first is the use of Eulerian statistics from DNS to examine and suggest improvements for model assumptions. The second is to use Lagrangian data from DNS to evaluate the performance of stochastic models in predicting Lagrangian quantities, such as autocorrelation functions, which are obtained by analyzing Lagrangian time series. A recent example of such a two-step effort was that of Sawford and Yeung[11,12] for the problem of velocity statistics in homogeneous shear flow. For the LSR model the first step has been reported in Vedula *et al.*;[13] the second is our focus in this paper. Improvements and new features reported here include improved modeling for the conditional diffusion term, which is the key unclosed quantity in Lagrangian PDF equations. As we demonstrate in the latter sections of this paper, good agreement is generally obtained at several different Reynolds numbers and Schmidt numbers.

The remaining sections of this paper are organized as follows. In Sec. II we provide background information on various elements of the LSR model formulation, including modified model assumptions based on Eulerian DNS results given in Vedula *et al.*[13] In Sec. III we introduce two alternative models for the conditional scalar diffusion of multiple scalars, based on white-noise and colored-noise processes. Although the white-noise version (which leads to a Fokker–Planck equation) is simpler, the colored-noise version is more realistic in that it allows for molecular diffusion effects having a finite correlation time. Comparisons with DNS data are given in Sec. IV, primarily in terms of auto- and cross-correlations of different flow variables. In Sec. V we summarize the results of this work and discuss implications for further model development. Given the importance of time correlation functions in the Lagrangian context, it is useful to note that analytical approximations can be derived. These are given in the Appendix.

## II. LAGRANGIAN PDF MODELS

### A. Problem formulation

We consider Lagrangian PDF mixing models needed to describe the Lagrangian DNS data presented in Yeung.[10] Lagrangian data available for isotropic turbulence with uniform mean scalar gradients include the following variables:

(i) $u^+(t)$, fluctuating velocity component in the direction of the mean scalar gradients;
(ii) $\epsilon^+(t)$, dissipation rate of turbulent kinetic energy;

TABLE I. Basic parameters from DNS.

| | | | | |
|---|---|---|---|---|
| Grid | $256^3$ | $256^3$ | $256^3$ | $512^3$ |
| $R_\lambda$ | 38 | 91 | 134 | 234 |
| $Sc$'s | 1/4,1 | 1/8,1 | 1/8,1 | 1/8,1 |
| $k/\langle\epsilon\rangle$ | 1.403 | 2.831 | 2.528 | 2.737 |

(iii) $\phi_\alpha^+(t)$, scalars ($\alpha$=1,2) with different Schmidt numbers ($Sc_1=1/8$, $Sc_2=1$);
(iv) $\chi_\alpha^+(t)\equiv 2D_\alpha(\nabla\phi_\alpha)^+\cdot(\nabla\phi_\alpha)^+$, scalar dissipation rates;
(v) $\chi_{12}^+(t)\equiv 2\sqrt{D_1D_2}(\nabla\phi_1)^+\cdot(\nabla\phi_2)^+$, joint scalar dissipation rate.

Due to stationarity, in the model the turbulent kinetic energy $k\equiv 3\langle u^2\rangle/2$ and the mean turbulence dissipation $\langle\epsilon\rangle$ are taken to be constant in time. Likewise, the Eulerian statistics of the scalar fields are treated as time independent. For this flow, the scalar mean values are equal: $\langle\phi_1\rangle=\langle\phi_2\rangle=Gx$, where $G$ is the uniform gradient, and the scalar fluctuations are nearly Gaussian. Nevertheless, the scalar variances and covariance are functions of the Schmidt and Reynolds numbers. Without loss of generality, in the model we will assume that the mean turbulence frequency $\langle\omega\rangle=\langle\epsilon\rangle/k=1$, and the velocity is normalized such that $\langle u^2\rangle=1$. Comparison with DNS data for dimensionless quantities (such as correlation functions) will only require renormalization of the time variable using the DNS turbulence frequency (see Table I). In other words, the time variable $t$ appearing in the model equations corresponds to the dimensionless time found using $\langle\omega\rangle$.

In the PDF model, the fluid–particle variables are represented by notional particles, whose properties are denoted by an asterisk. The notional particle position vector $\mathbf{X}^*(t)$ evolves by a modeled velocity, in the form

$$\frac{d\mathbf{X}^*}{dt}=\mathbf{u}^*(t). \tag{4}$$

In the flow under consideration, we can write the scalars as

$$\phi_\alpha^*(t)=\phi_\alpha'^*(t)+GX^*(t), \tag{5}$$

where $\phi_\alpha'^*(t)$ denotes the modeled scalar fluctuation, and $X^*$ is the component of $\mathbf{X}^*$ in the direction of the mean scalar gradient. The Lagrangian scalar increment over a small time interval $dt$ is given by

$$d\phi_\alpha^*=d\phi_\alpha'^*+GdX^*=d\phi_\alpha'^*+Gu^*dt. \tag{6}$$

Thus, by writing the model in terms of $\phi_\alpha'^*$, only the fluctuating velocity is needed to describe the scalar fields. Note that the mean scalar gradients are equal and collinear for the DNS data under consideration. However, this is not required: The model can be easily generalized[4] to uniform mean scalar gradients of arbitrary orientation and magnitude. Because the magnitudes of the mean scalar gradients affect only the magnitudes of the scalar fluxes and the scalar variance, but not the correlation functions nor other dimensionless statistics (see Appendix), we will set $G=1$ hereafter.

As noted in the Introduction, our principal modeling objective is to achieve both Eulerian and Lagrangian correspondence between the fluid–particle and notional–particle variables. For statistically stationary flow, the two-time statistics depend only on the time lag, $\tau$, and can be expressed in terms of Lagrangian correlation functions[10] $\rho^+(\tau)$. Thus, we will require that the Lagrangian PDF models agree with the DNS data at the level of two-time statistics: $\rho^*(\tau)=\rho^+(\tau)$. We should note here that none of the scalar mixing models presently available (e.g., IEM,[14] binomial,[15] EMST,[16] mapping closure[17]) satisfy Lagrangian correspondence. Indeed, only with the availability of Lagrangian DNS data is it now possible to validate this property. Moreover, because it requires the scalar time series $\phi_\alpha^*(t)$ to vary ''smoothly'' with time, the principle of Lagrangian correspondence should have significant impact on Lagrangian PDF predictions for reacting flows. For example, rapid variations in the Lagrangian scalars can lead to fluctuations that evolve faster than the characteristic response time of the flame chemistry. In contrast, slow variations of the same magnitude would allow the flame chemistry enough time to respond and thereby remain in chemical equilibrium. Thus, in order to capture accurately the dynamics of the interactions between mixing and chemistry, the modeled scalars should (as a minimum) achieve one-particle, two-time Lagrangian correspondence.

In summary, Lagrangian PDF models for $u^*(t)$, $\epsilon^*(t)$, $\phi_\alpha'^*(t)$, and $\chi_{\alpha\beta}^*(t)$ are required for comparison with DNS data. These models should satisfy both the Eulerian and Lagrangian correspondence criteria. Models for the scalars and scalar dissipation rate must also account for differential diffusion ($Sc_1\neq Sc_2$), including dependence on Reynolds number.

### B. Velocity

In isotropic turbulence, the velocity fluctuations are nearly Gaussian and the autocorrelation function approaches an exponential form for large Reynolds numbers.[10] Thus, in this work, we use a simple Langevin model[2] for $u^*(t)$:

$$du^*(t)=-\tfrac{3}{4}C_0u^*(t)dt+(\tfrac{3}{2}C_0)^{1/2}dW(t), \tag{7}$$

where $W(t)$ is a Gaussian white-noise process, and $C_0$ is the Kolmogorov constant in the second-order Lagrangian structure function. (Recall that the time $t$ has been made dimensionless using $\langle\omega\rangle$.) This model generates (see Appendix) a velocity time series with $\langle u^*(t)\rangle=0$, $\langle u^*(t)u^*(t)\rangle=1$, and autocorrelation function

$$\rho_u^*(\tau)=\exp(-\tfrac{3}{4}C_0|\tau|). \tag{8}$$

From this expression, the dimensionless Lagrangian velocity integral time scale $T_u$ (which is sometimes also denoted as $T_L$) defined to be $\int_0^\infty\rho_u^*(\tau)d\tau$ is given by $4/(3C_0)$. While $C_0$ is assumed to be an universal constant in the high Reynolds number limit, in comparisons with DNS data[10] it is best to allow for finite Reynolds numbers effects. In this work, we will fit $C_0$ to the DNS data for $T_u$ as a function of Reynolds number[18]

$$C_0 = 6.5\left[1 + \frac{8.1817}{R_\lambda}\left(1 + \frac{110}{R_\lambda}\right)\right]^{-1}, \tag{9}$$

where $R_\lambda$ is the Taylor-scale Reynolds number. Note that at very large Reynolds numbers, this expression gives $C_0 = 6.5$, which is consistent with recent estimates.[12,19,20]

### C. Turbulence frequency

The instantaneous turbulence frequency ($\omega \equiv \epsilon/k$) is important in the LSR model. In particular, it appears as the ''noise'' term in the model equations for the conditional scalar dissipation rates, and thus has a significant effect on the statistics of the scalar dissipation rates.[3] Based on DNS,[21] the one-point PDF of $\omega$ has a stretched-exponential form, with behavior at large $\omega$ depending on the Reynolds number. For a fixed turbulence kinetic energy in the model, fluctuations in $\omega$ are clearly proportional to those of the energy dissipation rate, for which Lagrangian statistics are also known from DNS.[10,22]

In the present paper we model the notional-particle turbulence frequency $\omega^*(t)$ using the stretched-exponential form suggested by Fox[3]

$$d\omega^*(t) = C_1\left(1 - \frac{(\omega^*(t))^{\gamma_1}}{\langle(\omega^*(t))^{1+\gamma_1}\rangle}\right)\omega^*(t)dt + \omega^*(t) \times \left(\frac{2C_1(1 + C_\omega\omega^*(t))}{3(\gamma_\omega + 0.5C_\omega\omega^*(t))}\right)^{1/2} dW(t), \tag{10}$$

where $\langle\omega^*(t)\rangle = 1$, and $\gamma_\omega$, $C_\omega$, and $\gamma_1$ are model parameters which control the shape of the PDF of $\omega$. In earlier work[3] $\gamma_\omega$ and $C_\omega$ were selected as 10/9 and 0.35, respectively. In particular, $\gamma_1$ determines the decay rate of the PDF for large $\omega$ and is known to decrease slowly with Reynolds number. Using DNS data[13] for the standardized moments of $\epsilon$, we find that a suitable power-law fit is

$$\gamma_1 = 1.25Re_1^{-0.26}, \tag{11}$$

where, using standard isotropy relations, we can write

$$Re_1 \equiv \frac{k}{\sqrt{\nu\langle\epsilon\rangle}} = 0.3873R_\lambda. \tag{12}$$

The autocorrelation time $T_\omega$ found from Eq. (10) is inversely proportional to $C_1$. The latter can be fit to the DNS data[10] as

$$C_1 = 2.54Re_1^{0.577}. \tag{13}$$

Note that $T_\omega$ decreases with increasing Reynolds number over the range of the DNS data ($38 \leqslant R_\lambda \leqslant 234$). If this trend continues for very large Reynolds numbers, the turbulence frequency could eventually be represented by a stretched-exponential white-noise process. As discussed elsewhere,[3] the autocorrelation time of $\omega^*$ has a direct effect on the conditional scalar dissipation rate $\langle\chi_\alpha|\epsilon\rangle$. Thus, as to be shown in Sec. IV, it may be necessary to modify Eq. (13) in order to accurately predict $\langle\chi_\alpha|\epsilon\rangle$.

### D. Scalars

In order to complete the Lagrangian PDF model, a closure is needed to describe the mixing of, in general, a set of (say) $N$ scalars, which are together called the composition vector, $\boldsymbol{\phi}'^*$. In our problem formulation the modeled value $\phi'^*_\alpha$ of each scalar evolves by the equation

$$\frac{d\phi'^*_\alpha}{dt} = \langle D_\alpha\nabla^2\phi'_\alpha|\boldsymbol{\phi}'^*\rangle^* - u^*(t)G, \tag{14}$$

for each of $\alpha = 1,2,...,N$. Here and elsewhere the notation $\langle\cdot|\phi^*\rangle^*$ denotes the expected value conditioned on both the scalars $\boldsymbol{\phi} = \boldsymbol{\phi}^*$ and the turbulence frequency $\{\epsilon = \epsilon^*(s), s \leqslant t\}$. (One should, in principle, also condition on the velocity.[23] However, for simplicity we will not do so here.) This equation can be written in a more compact vector form as

$$\frac{d\boldsymbol{\phi}'^*}{dt} = \langle\mathbf{D}\nabla^2\boldsymbol{\phi}'|\boldsymbol{\phi}^*\rangle^* - u^*(t)G\mathbf{1}, \tag{15}$$

where $\mathbf{1} \equiv [1,1\cdots1]^{\mathrm{T}}$ is a vector of all elements equal to unity, and the diagonal diffusion matrix is defined by

$$\mathbf{D} \equiv \mathbf{diag}(D_1,\ldots,D_N). \tag{16}$$

The molecular mixing term $\langle\mathbf{D}\nabla^2\boldsymbol{\phi}'|\boldsymbol{\phi}^*\rangle^*$ is unclosed and must be modeled.

For the case of Gaussian-distributed scalar fluctuations, the simplest linear model for the scalar-conditioned scalar diffusion can be written in matrix form as

$$\langle\mathbf{D}\nabla^2\boldsymbol{\phi}'|\boldsymbol{\phi}'\rangle = -\tfrac{1}{2}\mathbf{S}_D\boldsymbol{\chi}\mathbf{S}_D^{-1}\mathbf{C}^{-1}\boldsymbol{\phi}', \tag{17}$$

where $\mathbf{S}_D = \sqrt{\mathbf{D}}$, $\boldsymbol{\chi} \equiv [\langle\chi_{\alpha\beta}\rangle]$ is the scalar dissipation rate matrix, and $\mathbf{C} \equiv [\langle\phi'_\alpha\phi'_\beta\rangle]$ is the scalar covariance matrix. For the single-scalar case, Eq. (17) reduces to the well-known interaction-by-exchange-with-the-mean (IEM) model[6]

$$\langle D\nabla^2\phi'|\phi'\rangle^* = -\frac{\chi}{2\langle\phi'^2\rangle}\phi', \tag{18}$$

which has been verified in DNS.[5] With superscript T denoting a matrix transpose, the evolution of the scalar covariance matrix $\mathbf{C}$ can be written as

$$\begin{aligned}\frac{d\mathbf{C}}{dt} &= \left\langle\frac{d\boldsymbol{\phi}'}{dt}\boldsymbol{\phi}'^{\mathrm{T}}\right\rangle + \left\langle\frac{d\boldsymbol{\phi}'}{dt}\boldsymbol{\phi}'^{\mathrm{T}}\right\rangle^{\mathrm{T}} \\ &= \langle\langle\mathbf{D}\nabla^2\boldsymbol{\phi}'|\boldsymbol{\phi}'\rangle\boldsymbol{\phi}'^{\mathrm{T}}\rangle + \langle\langle\mathbf{D}\nabla^2\boldsymbol{\phi}'|\boldsymbol{\phi}'\rangle\boldsymbol{\phi}'^{\mathrm{T}}\rangle^{\mathrm{T}} \\ &\quad - G[\mathbf{1}\langle u^*\boldsymbol{\phi}'\rangle^{\mathrm{T}} + \langle u^*\boldsymbol{\phi}'\rangle\mathbf{1}^{\mathrm{T}}].\end{aligned} \tag{19}$$

Use of Eq. (17) for the conditional-diffusion terms on the right-hand side yields

$$\begin{aligned}&\langle\langle\mathbf{D}\nabla^2\boldsymbol{\phi}'|\boldsymbol{\phi}'\rangle\boldsymbol{\phi}'^{\mathrm{T}}\rangle + \langle\langle\mathbf{D}\nabla^2\boldsymbol{\phi}'|\boldsymbol{\phi}'\rangle\boldsymbol{\phi}'^{\mathrm{T}}\rangle^{\mathrm{T}} \\ &\quad = -\tfrac{1}{2}\mathbf{S}_D\boldsymbol{\chi}\mathbf{S}_D^{-1}\mathbf{C}^{-1}\langle\boldsymbol{\phi}'\boldsymbol{\phi}'^{\mathrm{T}}\rangle - \tfrac{1}{2}[\mathbf{S}_D\boldsymbol{\chi}\mathbf{S}_D^{-1}\mathbf{C}^{-1}\langle\boldsymbol{\phi}'\boldsymbol{\phi}'^{\mathrm{T}}\rangle]^{\mathrm{T}} \\ &\quad = -\tfrac{1}{2}\mathbf{S}_D\boldsymbol{\chi}\mathbf{S}_D^{-1} - \tfrac{1}{2}\mathbf{S}_D^{-1}\boldsymbol{\chi}\mathbf{S}_D = -[\delta_{\alpha\beta}\langle\chi_{\alpha\beta}\rangle],\end{aligned} \tag{20}$$

where

$$\delta_{\alpha\beta} \equiv \frac{1}{2}\left[\left(\frac{Sc_\alpha}{Sc_\beta}\right)^{1/2} + \left(\frac{Sc_\beta}{Sc_\alpha}\right)^{1/2}\right]. \tag{21}$$

The final term on the right-hand side of Eq. (20) thus gives the correct expression for the decay rate of the scalar covariance.[4]

Equation (17) cannot be used directly in situations where the matrix $\mathbf{C}$ is rank-deficient such that the matrix inverse $\mathbf{C}^{-1}$ does not exist. (This situation would arise when some of the scalars have the same diffusivities, so that they are not fully linearly independent.) This limitation can be overcome by extensions proposed in Sec. III. However, a more substantial shortcoming is that, as we also discuss in Sec. III, this simple model does not predict the correct behavior of the scalar autocorrelation functions. Thus, in this work, Eq. (17) is extended using two new closures described in Sec. III. One closure is based on the Fokker–Planck model[4] that uses a white-noise process with zero decorrelation time in the diffusion term. The other closure uses a colored-noise process with finite decorrelation time. We shall see that the latter yields scalar time series having smoother features that more closely resemble the DNS data. Both closures require information concerning a Lagrangian mixing time which is provided by the LSR model itself.

### E. LSR model

In order to model the scalar covariance matrix $\mathbf{C}$, we will employ the Lagrangian spectral relaxation (LSR) model.[3,4] For two scalars, the LSR model introduces the following Lagrangian conditional variables:

(i) $\langle \phi'_\alpha \phi'_\beta \rangle_i^*(t) \equiv \langle \phi'^*_\alpha(t) \phi'^*_\beta(t) | \epsilon^*(s), s \leqslant t \rangle_i$ with $\alpha, \beta = 1,2$, Lagrangian scalar variances/covariance in $i$th wavenumber band conditioned on the energy dissipation rate;

(ii) $\langle \phi'_\alpha \phi'_\beta \rangle^*(t) \equiv \Sigma_i \langle \phi'_\alpha \phi'_\beta \rangle_i^*(t)$, conditional Lagrangian scalar variances and covariances evaluated by summing over discrete wavenumber bands;

(iii) $\Phi_\alpha^*(t) \equiv \langle \phi'^2_\alpha \rangle^*(t) / \langle \phi'^2_\alpha \rangle$, conditional Lagrangian scalar variances normalized by unconditional values;

(iv) $\langle \chi_{\alpha\beta} \rangle^*(t) \equiv \langle \chi^*_{\alpha\beta}(t) | \epsilon^*(s), s \leqslant t \rangle$, Lagrangian scalar dissipation rates conditioned on energy dissipation. (Note that this is twice the quantity $\langle \epsilon_{\alpha\beta} \rangle^*$ in earlier work.[3,4])

Each of these variables will be discussed in more detail below. For now, we note that the scalars carried by each notional particle have their own characteristic mixing times

$$\tau_\alpha^\dagger(t) \equiv \frac{\langle \phi'^2_\alpha \rangle^*(t)}{\langle \chi_\alpha \rangle^*(t)}, \tag{22}$$

which depend on both Reynolds and Schmidt numbers. (As in earlier work,[3,4] a † is used to denote the ratio of two conditional quantities. Thus, for example, $\tau_\alpha \equiv \langle \phi'^2_\alpha \rangle / \langle \chi_\alpha \rangle$ is not the same as $\langle \tau_\alpha^\dagger \rangle$.) In order to compute the scalar-gradient source terms in the equation for the conditional scalar covariance, the LSR model requires as input the scalar fluxes $\langle u \phi'_\alpha \rangle$ and the scalar variances $\langle \phi'^2_\alpha \rangle$. These quantities are estimated from $u^*(t)$ and $\phi'^*_\alpha(t)$ using ensemble averages.

Conditional expected values of the form $\langle \cdot^*(t) | \epsilon^*(s), s \leqslant t \rangle$ account for the turbulence time history ($s \leqslant t$) experienced by the fluid particle. Unfortunately, their evaluation in DNS requires multiple simulations with the same velocity field but independent, identically distributed initial scalar fields—which incurs prohibitive computational costs. The related (although not equivalent) quantities $\langle \cdot^*(t) | \epsilon^*(t) \rangle$, which depend only on the current ($s = t$) energy dissipation are much easier to obtain. Eulerian conditional statistics such as, e.g., $\langle \chi_\alpha(\mathbf{x},t) | \epsilon(\mathbf{x},t) = \epsilon \rangle$ can be extracted from DNS[13] and compared with the corresponding Lagrangian conditional expected value $\langle \chi_\alpha^*(t) | \epsilon^*(t) = \epsilon \rangle$. Thus in this work we limit ourselves to conditioning only on current values of the energy dissipation.

An alternative method for estimating $\langle \chi_\alpha^*(t) | \epsilon^*(s), s \leqslant t \rangle$ can be formulated based on the Eulerian spatial correlation properties of the fluctuations of $\epsilon(\mathbf{x},t)$. In isotropic turbulence it is reasonable to expect that dissipation fluctuations at two points in space would remain strongly correlated only within a distance $L_\epsilon$ that scales with the Kolmogorov length scale $\eta$. Based on this argument, we can approximate $\langle \chi_\alpha^*(t) | \epsilon^*(s), s \leqslant t \rangle$ from DNS data by averaging the scalar-dissipation field $\chi_\alpha(\mathbf{x},t)$ over a sphere of diameter $L_\epsilon$ centered at $\mathbf{X}^+(t)$. Although this estimate would be accurate only for relatively large Schmidt numbers, the physical picture it provides is useful for understanding the structure of the scalar mixing model. In particular, the mixing times $\tau_\alpha^\dagger(t)$ correspond to values averaged over a volume with length scale $L_\epsilon$, as opposed to global averages [e.g., $\tau_\alpha(t)$] or instantaneous values [e.g., defined in terms of $\chi_\alpha^*(t)$].

A method for validating the model equations for the spectral transfer rates was developed by Fox and Yeung.[24] Because of stationarity, the spectral transfer rates appearing in the LSR model[4] have little effect on the Lagrangian time series. Nevertheless, because differential-diffusion effects are generated in the scalar-dissipation range and transferred to the inertial-convective and energy-containing ranges by backscatter, the multiscale description used in the LSR model is an integral part of the Lagrangian PDF mixing model.

In our recent work,[13] various terms in the LSR model equations for $\langle \chi_\alpha \rangle^*(t)$ and $\langle \phi'^2_\alpha \rangle^*(t)$ were validated and modified using DNS data for a range of Reynolds and Schmidt numbers. Specific changes to the original model[3] adopted in this paper include the following:

(i) The gradient-amplification constant $C_s$ is replaced by $C_s(\epsilon) = C_B(\epsilon) - C_D$ where the function $C_B(\epsilon)$ is given in the Appendix of Vedula *et al.*[13] The model for the gradient amplification term in the equation for $\langle \chi_\alpha \rangle^*(t)$ can be expressed as

$$-4 \left\langle \frac{\partial \phi'_\alpha}{\partial x_i} s_{ij} \frac{\partial \phi'_\alpha}{\partial x_j} \right\rangle^* = C_s(\omega^*(t)) \frac{\langle \omega \rangle}{Re_1} \sigma^*(t) \langle \chi_\alpha \rangle^*(t), \tag{23}$$

where the "noise" term is defined by

$$\sigma^*(t) = \frac{(\omega^*(t))^\gamma}{\langle (\omega^*(t))^\gamma \rangle}, \tag{24}$$

and the nominal value of the "stretching" exponent is $\gamma = 0.5$.

TABLE II. Parameters and spectral transfer functions in the LSR model.

$\gamma_1=(1-b)(1-a)(1-a/2)$ $\alpha_{12}=1/t_1$ $\beta_{12}=c_b\alpha_{12}$ $\beta_{21}=c_b(\alpha_{23}-\alpha_{12})$

$\gamma_2=a(1-b)(1-a/2)$ $\alpha_{23}=\alpha_{12}/a$ $\beta_{23}=c_b\alpha_{23}$ $\beta_{32}=c_b(\alpha_{3D}-\alpha_{12})$

$\gamma_3=a(1-b)/2$ $\alpha_{3D}=\alpha_{12}/c$ $\beta_{3D}=c_b\alpha_{3D}$ $\beta_{D3}=c_b\alpha_{12}Sc_{\alpha\beta}^{1/2}(1-b)/b$

$\gamma_D=b$ $\beta_\chi=c_bSc_{\alpha\beta}^{1/2}(1-b)$

$$a=1-\frac{1}{C_uRe_1} \quad b=\frac{2C_d}{1+C_BRe_1/R_0+\sqrt{(1+C_BRe_1/R_0)^2-4C_dC_DRe_1/R_0}}$$

$$c=\frac{aC_uRe_1+3(1-Sc_{\alpha\beta}^{-1/3})}{2C_uRe_1} \quad c_b=1 \quad R_0=\frac{k}{t_1\langle\epsilon\rangle} \quad Re_1=\frac{k}{\sqrt{\nu\langle\epsilon\rangle}}$$

$C_D=0.02$ $C_u=(0.1)^{2/3}=0.2154$ $C_B=1$ $C_d=3$

$$\mathcal{T}_1^*=\beta_{21}\langle\phi'_\alpha\phi'_\beta\rangle_2^*-(\alpha_{12}+\beta_{12})\langle\phi'_\alpha\phi'_\beta\rangle_1^*$$

$$\mathcal{T}_2^*=(\alpha_{12}+\beta_{12})(f_1\langle\phi'_\alpha\phi'_\beta\rangle_1^*+f_1^c\langle\phi'_\alpha\phi'_\beta\rangle_1)+\beta_{32}\langle\phi'_\alpha\phi'_\beta\rangle_3^*-(\alpha_{23}+\beta_{23})\langle\phi'_\alpha\phi'_\beta\rangle_2^*-\beta_{21}\langle\phi'_\alpha\phi'_\beta\rangle_2^*$$

$$\mathcal{T}_3^*=(\alpha_{23}+\beta_{23})(f_2\langle\phi'_\alpha\phi'_\beta\rangle_2^*+f_2^c\langle\phi'_\alpha\phi'_\beta\rangle_2)+\beta_{D3}\langle\phi'_\alpha\phi'_\beta\rangle_D^*-(\alpha_{3D}+\beta_{3D})\langle\phi'_\alpha\phi'_\beta\rangle_3^*-\beta_{32}\langle\phi'_\alpha\phi'_\beta\rangle_3^*$$

$$\mathcal{T}_D^*=(\alpha_{3D}+\beta_{3D})(f_3\langle\phi'_\alpha\phi'_\beta\rangle_3^*+f_3^c\langle\phi'_\alpha\phi'_\beta\rangle_3)-\beta_{D3}\langle\phi'_\alpha\phi'_\beta\rangle_D^*$$

$$\mathcal{T}_\chi^*=\delta_{\alpha\beta}^{-1}(\alpha_{3D}+\beta_{3D})(f_3\langle\phi'_\alpha\phi'_\beta\rangle_3^*+f_3^c\langle\phi'_\alpha\phi'_\beta\rangle_3)-\beta_\chi\langle\chi_{\alpha\beta}\rangle^*$$

$$f_1=\left(\frac{1}{C_uRe_1}\right)^{3/2} \quad f_2=\left(\frac{3}{C_uRe_1+2}\right)^{3/2} \quad f_3=\sqrt{Sc_{\alpha\beta}}$$

$$f_n^c=1-f_n \quad f_D=1-\exp\left(-\frac{0.466}{\sqrt{Sc_{\alpha\beta}}}\right)$$

Notes:
(i) $\gamma_1+\gamma_2+\gamma_3+\gamma_D=1$.
(ii) Only the parameters for the scalar-dissipation range depend on the Schmidt number $Sc_{\alpha\beta}$.
(iii) An $\omega^*$-dependent form of $C_d$ is used in Eq. (29).
(iv) The model is defined for values of $Re_1$ and $Sc_{\alpha\beta}\leqslant 1$ such that are all parameters are positive.
(v) The parameter $t_1$ is fixed to match $r_\phi$ from the DNS as described in Sec. II.

(ii) The molecular-dissipation constant $C_d$ is replaced by the function $C_d(\epsilon)$ given in the Appendix of Vedula *et al.*[13]

(iii) The molecular-dissipation term in the equation for $\langle\phi'^2_\alpha\rangle^*(t)$ is modified to include Schmidt-number dependence for the quantity $f_D^*$ as described in Vedula *et al.*[13]

Separate work[25] has suggested that these modifications are also valid for model equations for the two-scalar variables [i.e., $\langle\chi_{12}\rangle^*(t)$ and $\langle\phi'_1\phi'_2\rangle^*(t)$]. For the covariance equations, an equivalent Schmidt number ($Sc_{\alpha\beta}\equiv\nu/D_{\alpha\beta}$) is defined using the average diffusivity $D_{\alpha\beta}\equiv(D_\alpha+D_\beta)/2$.

Using as an example a case with four wavenumber bands (denoted by subscripts 1, 2, 3, and $D$), the LSR model for the scalar variances in each wavenumber band is given by

$$\frac{\mathrm{d}\langle\phi'_\alpha\phi'_\beta\rangle_1^*}{\mathrm{d}t}=\mathcal{T}_1^*+\gamma_1\mathcal{P}_{\alpha\beta}+\frac{\gamma_D\delta_{\alpha\beta}\langle\chi_{\alpha\beta}\rangle}{\langle\phi'_\alpha\phi'_\beta\rangle_D}(\langle\phi'_\alpha\phi'_\beta\rangle_1-\langle\phi'_\alpha\phi'_\beta\rangle_1^*)+f_D\delta_{\alpha\beta}\left(\langle\chi_{\alpha\beta}\rangle^*\frac{\langle\phi'_\alpha\phi'_\beta\rangle_1}{\langle\phi'_\alpha\phi'_\beta\rangle}-\langle\chi_{\alpha\beta}\rangle\frac{\langle\phi'_\alpha\phi'_\beta\rangle_1^*}{\langle\phi'_\alpha\phi'_\beta\rangle}\right), \tag{25}$$

$$\frac{\mathrm{d}\langle\phi'_\alpha\phi'_\beta\rangle_2^*}{\mathrm{d}t}=\mathcal{T}_2^*+\gamma_2\mathcal{P}_{\alpha\beta}+\frac{\gamma_D\delta_{\alpha\beta}\langle\chi_{\alpha\beta}\rangle}{\langle\phi'_\alpha\phi'_\beta\rangle_D}(\langle\phi'_\alpha\phi'_\beta\rangle_2-\langle\phi'_\alpha\phi'_\beta\rangle_2^*)+f_D\delta_{\alpha\beta}\left(\langle\chi_{\alpha\beta}\rangle^*\frac{\langle\phi'_\alpha\phi'_\beta\rangle_2}{\langle\phi'_\alpha\phi'_\beta\rangle}-\langle\chi_{\alpha\beta}\rangle\frac{\langle\phi'_\alpha\phi'_\beta\rangle_2^*}{\langle\phi'_\alpha\phi'_\beta\rangle}\right), \tag{26}$$

$$\frac{\mathrm{d}\langle\phi'_\alpha\phi'_\beta\rangle_3^*}{\mathrm{d}t}=\mathcal{T}_3^*+\gamma_3\mathcal{P}_{\alpha\beta}+\frac{\gamma_D\delta_{\alpha\beta}\langle\chi_{\alpha\beta}\rangle}{\langle\phi'_\alpha\phi'_\beta\rangle_D}(\langle\phi'_\alpha\phi'_\beta\rangle_3-\langle\phi'_\alpha\phi'_\beta\rangle_3^*)+f_D\delta_{\alpha\beta}\left(\langle\chi_{\alpha\beta}\rangle^*\frac{\langle\phi'_\alpha\phi'_\beta\rangle_3}{\langle\phi'_\alpha\phi'_\beta\rangle}-\langle\chi_{\alpha\beta}\rangle\frac{\langle\phi'_\alpha\phi'_\beta\rangle_3^*}{\langle\phi'_\alpha\phi'_\beta\rangle}\right), \tag{27}$$

and

$$\frac{\mathrm{d}\langle\phi'_\alpha\phi'_\beta\rangle_D^*}{\mathrm{d}t}=\mathcal{T}_D^*+\gamma_D\mathcal{P}_{\alpha\beta}+\frac{\gamma_D\delta_{\alpha\beta}\langle\chi_{\alpha\beta}\rangle}{\langle\phi'_\alpha\phi'_\beta\rangle_D}(\langle\phi'_\alpha\phi'_\beta\rangle_D-\langle\phi'_\alpha\phi'_\beta\rangle_D^*)+f_D\delta_{\alpha\beta}\left(\langle\chi_{\alpha\beta}\rangle^*\frac{\langle\phi'_\alpha\phi'_\beta\rangle_D}{\langle\phi'_\alpha\phi'_\beta\rangle}-\langle\chi_{\alpha\beta}\rangle\frac{\langle\phi'_\alpha\phi'_\beta\rangle_D^*}{\langle\phi'_\alpha\phi'_\beta\rangle}\right)-\delta_{\alpha\beta}\langle\chi_{\alpha\beta}\rangle^*, \tag{28}$$

where the covariance production term is $\mathcal{P}_{\alpha\beta}=-(\langle\phi'_\alpha u\rangle+\langle\phi'_\beta u\rangle)G$ (recall that $G=1$ is the uniform scalar gradient), and the spectral transfer rates $\mathcal{T}_i^*$ and other model parameters are given in Table II. The LSR model equation for the conditional two-scalar joint dissipation rate is

$$\frac{\mathrm{d}\langle\chi_{\alpha\beta}\rangle^*}{\mathrm{d}t}=\mathcal{P}_\chi+\frac{\gamma_D\delta_{\alpha\beta}\langle\chi_{\alpha\beta}\rangle}{\langle\phi'_\alpha\phi'_\beta\rangle_D}(\langle\chi_{\alpha\beta}\rangle-\langle\chi_{\alpha\beta}\rangle^*)+C_D\langle\omega\rangle Re_1\mathcal{T}_\chi^*+C_s(\omega^*)\langle\omega\rangle Re_1\sigma^*(t)\times\langle\chi_{\alpha\beta}\rangle^*-C_d(\omega^*)\frac{\delta_{\alpha\beta}\langle\chi_{\alpha\beta}\rangle^*}{\langle\phi'_\alpha\phi'_\beta\rangle_D^*}\langle\chi_{\alpha\beta}\rangle^*, \quad (29)$$

where

$$\mathcal{P}_\chi=-\frac{\gamma_D}{\delta_{\alpha\beta}}\left(\frac{\langle\chi_\alpha\rangle^*}{\langle\phi'^2_\alpha\rangle_D^*}\langle\phi'_\alpha u\rangle+\frac{\langle\chi_\beta\rangle^*}{\langle\phi'^2_\beta\rangle_D^*}\langle\phi'_\beta u\rangle\right)G. \quad (30)$$

Note that the only stochastic component in the LSR model comes from the gradient-amplification term involving $\sigma^*(t)$ in Eq. (29). The last three terms on the right-hand side of Eq. (29) are order $Re_1$, and thus are the dominant terms at high Reynolds numbers.

Summing together Eqs. (25)–(28) yields the LSR model equation for the conditional scalar covariance

$$\frac{\mathrm{d}\langle\phi'_\alpha\phi'_\beta\rangle^*}{\mathrm{d}t}=V_{\alpha\beta}^*+\mathcal{P}_{\alpha\beta}-\delta_{\alpha\beta}\langle\chi_{\alpha\beta}\rangle^*, \quad (31)$$

where the spectral transfer term is defined by

$$\begin{aligned}V_{\alpha\beta}^*\equiv&(\alpha_{12}+\beta_{12})f_1^c(\langle\phi'_\alpha\phi'_\beta\rangle_1-\langle\phi'_\alpha\phi'_\beta\rangle_1^*)\\&+(\alpha_{23}+\beta_{23})f_2^c(\langle\phi'_\alpha\phi'_\beta\rangle_2-\langle\phi'_\alpha\phi'_\beta\rangle_2^*)\\&+(\alpha_{3D}+\beta_{3D})f_3^c(\langle\phi'_\alpha\phi'_\beta\rangle_3-\langle\phi'_\alpha\phi'_\beta\rangle_3^*)\\&+\frac{\gamma_D\delta_{\alpha\beta}\langle\chi_{\alpha\beta}\rangle}{\langle\phi'_\alpha\phi'_\beta\rangle_D}(\langle\phi'_\alpha\phi'_\beta\rangle-\langle\phi'_\alpha\phi'_\beta\rangle^*)\\&+f_D\delta_{\alpha\beta}\left(\langle\chi_{\alpha\beta}\rangle^*-\langle\chi_{\alpha\beta}\rangle\frac{\langle\phi'_\alpha\phi'_\beta\rangle^*}{\langle\phi'_\alpha\phi'_\beta\rangle}\right).\end{aligned} \quad (32)$$

In general, $\langle\phi'_\alpha\phi'_\beta\rangle^*$ will be larger than $\langle\phi'_\alpha\phi'_\beta\rangle$ when $\langle\chi_{\alpha\beta}\rangle^*$ is smaller than $\langle\chi_{\alpha\beta}\rangle$, and vice versa. The role of $V_{\alpha\beta}^*$ is thus to transfer scalar variance from particles with low scalar dissipation rates to particles with high scalar dissipation rates. On average, the net transfer of scalar variance is null, i.e., $\langle V_{\alpha\beta}^*\rangle=0$.

As can be seen in Table II, the parameters in the LSR model depend on the Reynolds and Schmidt numbers. Also note that the characteristic time scale for the scalar-dissipation range (e.g., $\langle\phi'_\alpha\phi'_\beta\rangle_D^*/\langle\chi_{\alpha\beta}\rangle^*$) will be proportional to $R_\lambda^{-1}$. In comparison, the time scale for the turbulence frequency is, within the range of available DNS data, approximately proportional to $R_\lambda^{-0.577}$. This difference implies that the noise term [Eq. (24)] in the LSR model for the scalar dissipation rates will fluctuate with a shorter time scale than $\langle\chi_{\alpha\beta}\rangle^*(t)$. Consequently $\langle\chi_{\alpha\beta}\rangle^*(t)$ and $\omega^*(t)$ will remain highly correlated for very large Reynolds numbers, even as $\omega^*(t)$ approaches a white-noise process in this limit. In comparison, ''spectral-equilibrium'' models for the scalar dissipation rate (e.g., Sanders and Gökalp[26]) do not attempt to model the terms in the equation for $\langle\chi_\alpha\rangle$ directly, but instead the scalar flux through the inertial-convective range.[6] Such models cannot predict the instantaneous scalar dissipation rates, nor their dependence on small-scale processes (e.g., turbulence-frequency fluctuations or chemical reactions).

For the two-scalar mixing problem considered in this work, the scalar mixing model uses the normalized conditional variance ratios $\Phi_1^*(t)$, $\Phi_2^*(t)$ and the conditional scalar dissipation rates, $\langle\chi_1\rangle^*(t)$, $\langle\chi_{12}\rangle^*(t)$ and $\langle\chi_2\rangle^*(t)$ as input model parameters. In the limit of $Sc_1=Sc_2$ we recover the result of perfect correlation

$$\Phi_1^*(t)=\Phi_2^*(t), \quad (33)$$

$$\rho_{12}^\dagger(t)\equiv\frac{\langle\phi'_1\phi'_2\rangle^*(t)}{\sqrt{\langle\phi'^2_1\rangle^*(t)\langle\phi'^2_2\rangle^*(t)}}=1, \quad (34)$$

and

$$g_{12}^\dagger(t)\equiv\frac{\langle\chi_{12}\rangle^*(t)}{\sqrt{\langle\chi_1\rangle^*(t)\langle\chi_2\rangle^*(t)}}=1. \quad (35)$$

When $Sc_1\neq Sc_2$, the scalar-gradient correlation function $g_{12}^\dagger(t)$ will be nearly equal to the geometric-to-arithmetic-average molecular-diffusivity ratio, whereas the scalar correlation function $\rho_{12}^\dagger(t)$ will approach unity with increasing Reynolds number.[4,5] In terms of the Lagrangian scalar time series, mixing models for $\phi_1'^*(t)$ and $\phi_2'^*(t)$ must be capable of predicting the dependence of $\rho_{12}^\dagger(t)$ and $g_{12}^\dagger(t)$ on Reynolds and Schmidt numbers.

Finally, we note that the spectral transfer rates appearing in the LSR model were chosen to correspond to a high-Reynolds-number, fully developed model energy spectrum.[27] A key parameter is the spectral-transfer time scale from the energy-containing range to the inertial-convective range,[27] denoted by $t_1$. Based on the assumption that the Obukhov–Corrsin constant is independent of Reynolds number, the steady-state scalar time scale $(\langle\phi'^2\rangle/\langle\chi\rangle)$ for $Sc=1$ predicted by the model is equal to $t_1/2$. (Note that this assumption can be relaxed by making $t_1$ a function of Reynolds number as done below.) Thus, the mechanical-to-scalar time scale ratio

$$r_\phi=\frac{k/\langle\epsilon\rangle}{\langle\phi'^2\rangle/\langle\chi\rangle}, \quad (36)$$

is determined by the value of $t_1$. In the original model,[27] $t_1=k/\langle\epsilon\rangle$ was employed so that $r_\phi=2$ when $Sc=1$. However, in DNS the value of $r_\phi$ varies weakly with both Reynolds number and Schmidt number. Thus, in order to make valid comparisons with the DNS data, in this work we set $t_1$ for each Reynolds number by using the DNS value of $r_\phi$ for $Sc=1$ (see Table IV). All other spectral-transfer time scales are then expressed in terms of $t_1$ as described elsewhere.[4]

## III. LAGRANGIAN MODELS FOR SCALARS

In order to describe the fluctuating scalars $\boldsymbol{\phi}'^*(t)$, a closure is required for the conditional diffusion based on the Laplacian appearing in Eq. (15), with care taken to ensure

consistency with the LSR model predictions for the conditional scalar covariances $\langle \phi'_\alpha \phi'_\beta \rangle^*$. The choice of the closure, however, is not unique, and we will explore two alternative schemes below. The forms of these closures are mainly motivated by the desire to use the simplest possible model that yields good agreement with DNS. Thus, for example, the first (simplest) of these adequately predicts the Lagrangian scalar integral autocorrelation times, but not the detailed functional form of the autocorrelation functions themselves. We are, therefore, led to introduce a slightly more complicated model to correct this deficiency. Despite the improvement obtained, it should be noted that good agreement with other, more detailed, DNS statistics (e.g., especially two-scalar quantities, like those of the difference $\phi_1'^* - \phi_2'^*$) may require additional modifications. However, agreement at the level of the Lagrangian autocorrelation function should be sufficient for modeling extinction and reignition events in nonpremixed turbulent reacting flows. (For recent work on using DNS to model these complex nonequilibrium effects one may refer to Cha *et al.*[28])

In the two mixing models introduced below, a number of conditional statistics appear, and are supplied by the LSR model. For example, the conditional scalar dissipation rate matrix $\boldsymbol{\chi}^*$ determines the mixing time scales and ultimately the scalar correlation. Moreover, due to fluctuations in $\omega^*(t)$, $\boldsymbol{\chi}^*$ will be a random process with a different value for each notional particle. Likewise, the conditional scalar covariance matrix $\mathbf{C}^*$ is also supplied by the LSR model, and will be different for each notional particle. In the numerical implementation, unconditional statistics such as $\boldsymbol{\chi}$ and $\mathbf{C}$ are found by averaging over all notional particles. Thus, in general, any quantity with a superscript * will be carried by the notional particles, while the corresponding quantity without a superscript is found by ensemble averaging over all notional particles.

Finally, note that neither mixing model requires knowledge of the *instantaneous* joint scalar dissipation rates $\chi^*_{\alpha\beta}(t)$. Nevertheless, in order to make comparisons with DNS data, we provide a simple model for $\chi^*_{\alpha\beta}(t)$ at the end of this section that is consistent with the LSR model for $\boldsymbol{\chi}^*$ (i.e., the conditional expectation of the former is equal to the latter). As noted earlier, $\boldsymbol{\chi}^*(t)$ corresponds to the average scalar dissipation rate over a volume of fluid with nearly uniform $\epsilon(\mathbf{x},t)$, i.e., over a volume whose characteristic linear size is close to the Kolmogorov length scale. Inside this volume, large fluctuations in $\chi^*_{\alpha\beta}(t)$ will still be present. However, when describing the effect of the fluctuating strain field on local extinction and reignition events in turbulent reacting flows, fluctuations in $\boldsymbol{\chi}^*(t)$ should be more relevant than point-wise fluctuations in $\chi^*_{\alpha\beta}(t)$. Although we do not present typical time series for the components of $\boldsymbol{\chi}^*(t)$ here, it should be noted that their fluctuations can be quite large and sustained (e.g., values 2 to 3 times of the mean scalar dissipation rate are not uncommon). Such large variations in the scalar mixing time would be more than adequate to cause extinction in nonpremixed flames at moderate Damköhler numbers.

### A. Lagrangian Fokker–Planck model

The general form for the Lagrangian Fokker–Planck (LFP) model[29] is

$$\langle \mathbf{D}\nabla^2 \boldsymbol{\phi}' \,|\, \boldsymbol{\phi}^* \rangle^* \mathrm{d}t = -\tfrac{1}{2}\mathbf{M}^* \boldsymbol{\phi}'^* \mathrm{d}t + \mathbf{B}^*(\boldsymbol{\phi}^*)\mathrm{d}\mathbf{W}(t), \tag{37}$$

where the matrix coefficients $\mathbf{M}^*$ and $\mathbf{B}^*$ represent drift and diffusion terms, respectively, and $\mathbf{W}(t)$ is a multivariate Gaussian white-noise process. The matrix $\mathbf{B}^*(\boldsymbol{\phi}^*)$ is defined such that

$$\mathbf{B}^*(\boldsymbol{\phi}^*)\mathbf{B}^*(\boldsymbol{\phi}^*)^{\mathrm{T}} = C_2 \langle \boldsymbol{\chi} | \boldsymbol{\phi}^* \rangle^*, \tag{38}$$

where $C_2 = 1$ and the conditional scalar dissipation rate matrix is given by

$$\langle \boldsymbol{\chi} | \boldsymbol{\phi}^* \rangle^* \equiv [\langle \chi_{\alpha\beta} | \boldsymbol{\phi}^* \rangle^*]. \tag{39}$$

The drift matrix $\mathbf{M}^*$ adopted in this work can be written as

$$\mathbf{M}^* \equiv (\mathbf{S}_D \boldsymbol{\chi}^* \mathbf{S}_D^{-1} - \mathbf{V}^* + C_2 \boldsymbol{\chi}^*)\mathbf{S}_\phi^{-1}\mathbf{U}_\rho \boldsymbol{\Lambda}_\rho^{-1}\mathbf{U}_\rho^{\mathrm{T}}\mathbf{S}_\phi^{-1}. \tag{40}$$

Here some of the matrices on the right-hand side have simple definitions, as

$$\mathbf{S}_D \equiv \mathbf{diag}(\sqrt{D_1}, \ldots, \sqrt{D_N}), \tag{41}$$

$$\boldsymbol{\chi}^* \equiv [\langle \chi_{\alpha\beta} \rangle^*], \tag{42}$$

$$\mathbf{S}_\phi \equiv \mathbf{diag}(\sqrt{\langle \phi_1'^2 \rangle^*}, \ldots, \sqrt{\langle \phi_N'^2 \rangle^*}). \tag{43}$$

In addition, as described below, the symmetric matrix $\mathbf{V}^*$ [defined by Eq. (32)] describes the relaxation of the conditional scalar covariances towards their unconditional counterparts, whereas the orthonormal matrix $\mathbf{U}_\rho$ and diagonal matrix $\boldsymbol{\Lambda}_\rho$ are found from the eigenvalues and eigenvectors of the scalar correlation matrix $\boldsymbol{\rho}^\dagger \equiv [\rho^\dagger_{\alpha\beta}]$.

The matrix $\boldsymbol{\Lambda}_\rho$ is introduced to handle the case where the conditional scalar covariance matrix $\mathbf{C}^* \equiv [\langle \phi'_\alpha \phi'_\beta \rangle^*]$ is rank deficient. In cases where $\mathbf{C}^*$ is full rank, $\boldsymbol{\rho}^\dagger = \mathbf{U}_\rho \boldsymbol{\Lambda}_\rho \mathbf{U}_\rho^{\mathrm{T}}$ and $\mathbf{M}^*$ can be written more simply as

$$\mathbf{M}^* \equiv (\mathbf{S}_D \boldsymbol{\chi}^* \mathbf{S}_D^{-1} - \mathbf{V}^* + C_2 \boldsymbol{\chi}^*)\mathbf{C}^{*-1} \quad \text{if } \mathrm{rank}(\mathbf{C}^*) = N. \tag{44}$$

Note that, except for the conditioning on energy dissipation, this form of $\mathbf{M}^*$ agrees with the linear model given by Eq. (17) in the limit $C_2 = 0$.

The definition of the diffusion coefficient $\mathbf{B}^*$ is partly dictated by the requirement that the scalars remain bounded.[29] Indeed, for points on the boundary of the allowable region in composition space, the probability flux (i.e., the flux of the joint composition PDF) in the direction normal to the boundary must be zero. If we denote the boundary-normal vector at the point $\boldsymbol{\phi}_b$ on the boundary by $\mathbf{n}_b(\boldsymbol{\phi}_b)$, then from the theory of Fokker–Planck equations[30] it suffices to require that $\langle \boldsymbol{\chi} | \boldsymbol{\phi}_b \rangle^* \mathbf{n}_b(\boldsymbol{\phi}_b) = 0$ [i.e., the diffusive flux in the direction $\mathbf{n}_b(\boldsymbol{\phi}_b)$ must be null]. For general turbulent reacting flows, the functional dependence of the normal vector on $\boldsymbol{\phi}_b$ will be nontrivial. However, for the special case of nonpremixed nonreacting scalars (i.e., mixing between two or more streams with different concentrations),

the surfaces of the allowable region are hyperplanes so that $\mathbf{n}_b$ will be constant on each surface. A example for this case is discussed in Sec. V.

The form of the drift matrix $\mathbf{M}^*$ is set by the requirement that the conditional scalar covariance matrix agrees with the LSR model. In the absence of mean scalar gradients (i.e., with $G=0$), the LFP model yields

$$\frac{d\mathbf{C}^*}{dt} = -\frac{1}{2}[\mathbf{M}^*\mathbf{C}^* + \mathbf{C}^*\mathbf{M}^{*T}] + C_2\boldsymbol{\chi}^* = \mathbf{V}^* - [\delta_{\alpha\beta}\langle\chi_{\alpha\beta}\rangle^*], \tag{45}$$

where we have used Eq. (44) to simplify the product $\mathbf{M}^*\mathbf{C}^*$. The LSR model also provides an expression for $\mathbf{C}^*$ [Eq. (31)]. For the same conditions, the scalar covariance obeys Eq. (20). The matrix $\mathbf{V}^*$ thus controls the rate of decay of the difference

$$\frac{d(\mathbf{C}^*-\mathbf{C})}{dt} = \mathbf{V}^* + [\delta_{\alpha\beta}(\langle\chi_{\alpha\beta}\rangle - \langle\chi_{\alpha\beta}\rangle^*)]. \tag{46}$$

Note that, to ensure consistency, the expected value of the difference must be zero so that $\langle\mathbf{V}^*\rangle=\mathbf{0}$.

The definitions of $\boldsymbol{\Lambda}_\rho$ in terms of the eigenvalues of $\boldsymbol{\rho}^\dagger$ can only be used when $\mathbf{C}^*$ is full rank. This would not be the case, for example, if some of the scalars were perfectly correlated so that some of the eigenvalues would be null. It is thus necessary to define $\boldsymbol{\Lambda}_\rho$ such that the LFP model can be applied when $\mathbf{C}^*$ is rank deficient. We do this by using the eigenvalues of the conditional scalar correlation matrix $\boldsymbol{\rho}^\dagger$ and its orthonormal eigenvector matrix.[29] (Recall that $\boldsymbol{\rho}^\dagger$ is available from the LSR model.) It then follows that

$$\boldsymbol{\Lambda}_\rho \equiv \mathbf{diag}(\lambda_1,\ldots,\lambda_R,1,...,1) \tag{47}$$

where $\lambda_1,\ldots,\lambda_R$ are the nonzero eigenvalues of $\boldsymbol{\rho}^\dagger$ and the remaining zero eigenvalues have been replaced by ones. The matrix $\mathbf{U}_\rho$ is defined as the corresponding orthonormal eigenvector matrix. Using this decomposition for the two-scalar case, $\boldsymbol{\rho}^\dagger$ can be written as

$$\boldsymbol{\rho}^\dagger = \frac{1}{2}\begin{bmatrix}1 & 1\\ 1 & -1\end{bmatrix}\begin{bmatrix}1+\rho_{12}^\dagger & 0\\ 0 & 1-\rho_{12}^\dagger\end{bmatrix}\begin{bmatrix}1 & 1\\ 1 & -1\end{bmatrix} = \mathbf{U}_\rho\boldsymbol{\Lambda}_\rho\mathbf{U}_\rho^T. \tag{48}$$

(The second equality holds only when $|\rho_{12}^\dagger|\neq 1$.) The two eigenvalues are thus

$$\lambda_1 = 1+\rho_{12}^\dagger \quad \text{and} \quad \lambda_2 = 1-\rho_{12}^\dagger, \tag{49}$$

where $\lambda_2$ vanishes if the scalars are perfectly correlated. When this occurs, the rank of $\mathbf{C}^*$ is one and $\lambda_2$ can be replaced by any nonzero value (i.e., so that $\boldsymbol{\Lambda}_\rho$ can be inverted) without affecting the covariance matrix. Numerically, this replacement is implemented whenever $|\rho_{12}^\dagger| \geqslant 1-\epsilon_s$ where $0<\epsilon_s\ll 1$.

In order to use the LFP model, appropriate functional forms are needed for the scalar-conditioned scalar dissipation rates $\langle\chi_{\alpha\beta}|\boldsymbol{\phi}^*\rangle^*$. In general, these functions control the characteristic time scales for the scalars and the shape of the joint composition PDF.[29] For reacting scalars, they will be functions of the chemical source terms and hence difficult to model *a priori*. However, for the base case of passive and Gaussian-distributed scalar fluctuations, the scalar dissipation rates are statistically independent of the scalar fluctuation:[31] i.e., $\langle\chi_{\alpha\beta}|\boldsymbol{\phi}^*\rangle^* = \langle\chi_{\alpha\beta}\rangle^*$. Since the latter is available from the LSR model, for the DNS data under consideration, the diffusion matrix can be written as

$$\mathbf{B}^*(\boldsymbol{\phi}^*)\mathbf{B}^*(\boldsymbol{\phi}^*)^T = \begin{bmatrix}\sqrt{\langle\chi_1\rangle^*} & 0\\ 0 & \sqrt{\langle\chi_2\rangle^*}\end{bmatrix}\begin{bmatrix}1 & g_{12}^\dagger\\ g_{12}^\dagger & 1\end{bmatrix}\times\begin{bmatrix}\sqrt{\langle\chi_1\rangle^*} & 0\\ 0 & \sqrt{\langle\chi_2\rangle^*}\end{bmatrix}, \tag{50}$$

or, by using an eigenvalue decomposition of the correlation matrix, as

$$\mathbf{B}^*(\boldsymbol{\phi}^*) = \frac{1}{\sqrt{2}}\begin{bmatrix}\sqrt{\langle\chi_1\rangle^*} & 0\\ 0 & \sqrt{\langle\chi_2\rangle^*}\end{bmatrix}\times\begin{bmatrix}\sqrt{1+g_{12}^\dagger} & \sqrt{1-g_{12}^\dagger}\\ \sqrt{1+g_{12}^\dagger} & -\sqrt{1-g_{12}^\dagger}\end{bmatrix}. \tag{51}$$

Note that the characteristic time scale for each scalar is determined by $\langle\chi_\alpha\rangle^*$. Furthermore, in the case of perfectly correlated scalars with $|g_{12}^\dagger|=1$, the diffusion matrix is of rank one. The noise term in the LFP model will then be identical for both scalars, thereby preserving perfect correlation (i.e., the joint Gaussian PDF will be nonzero over a one-dimensional subspace in two-dimensional composition space). On the other hand, for $Sc_1\neq Sc_2$ the scalars will not be perfectly correlated and $|g_{12}^\dagger|<1$. In this case, the diffusion matrix is full rank and the joint Gaussian PDF will be nonzero over a two-dimensional space.

The LFP model in Eq. (37) has the form of a multivariate Ornstein–Uhlenbeck process with time-dependent coefficients.[30] The resulting matrix correlation function $\boldsymbol{\rho}_\phi(\tau)$ thus decays approximately (see Appendix) as an exponential with the eigenvalues of $\mathbf{M}^*$ determining the autocorrelation times. However, in reality, since the Lagrangian scalar time series should be differentiable, its autocorrelation function for small $|\tau|$ should have (as in DNS[10]) a quadratic shape with zero slope at the origin ($\tau=0$). Thus, although the LFP model yields good agreement with DNS for the integral scalar autocorrelation times, the predicted shapes of the autocorrelation functions are incorrect. (This difference is most clearly seen in the degree of ''smoothness'' of the scalar time series.) The problem lies in the use of the white-noise process $\mathbf{W}(t)$ in the LFP model. This thus provides motivation for a modified model that uses colored noise, as described in the next subsection.

### B. Lagrangian colored-noise model

In order to improve predictions of the scalar time series, a ''diffusion'' term with nonzero autocorrelation time is required. The Lagrangian colored-noise (LCN) model has the same form as the LFP model, but with a differentiable ''noise'' term

$$\langle \mathbf{D}\nabla^2\boldsymbol{\phi}'|\boldsymbol{\phi}^*\rangle^* = -\tfrac{1}{2}(\mathbf{S}_D\boldsymbol{\chi}^*\mathbf{S}_D^{-1} - \mathbf{V}^* + C_2\mathbf{S}_\chi\mathbf{D}^*\mathbf{S}_\chi)\mathbf{S}_\phi^{-1}\mathbf{U}_\rho\boldsymbol{\Lambda}_\rho^{-1}\mathbf{U}_\rho^{\mathrm{T}}\mathbf{S}_\phi^{-1}\boldsymbol{\phi}'^* + \tfrac{1}{2}C_2\langle\boldsymbol{\chi}|\boldsymbol{\phi}^*\rangle^*\mathbf{S}_\phi^{-1}\mathbf{h}^*(t), \tag{52}$$

where

$$\mathbf{S}_\chi \equiv \mathbf{diag}(\sqrt{\langle\chi_1\rangle^*},\ldots,\sqrt{\langle\chi_N\rangle^*}), \tag{53}$$

$\mathbf{D}^*$ is a symmetric positive-definite matrix defined such that the model yields the correct scalar dissipation rates, and $\mathbf{h}^*(t)$ is a Gaussian random vector. The components of $\mathbf{h}^*(t)$ are defined by

$$\mathrm{d}h_\alpha^* = -\frac{C_3}{2\tau_\alpha^\dagger(t)}h_\alpha^*\mathrm{d}t + \left(\frac{C_3}{\tau_\alpha^\dagger(t)}\right)^{1/2}\mathrm{d}W_\alpha(t), \tag{54}$$

where $\langle\mathbf{h}^*\rangle = 0$ and $\langle\mathbf{h}^*\mathbf{h}^{*\mathrm{T}}\rangle = \mathrm{I}$. Note that, like Eq. (7), Eq. (54) has the form of a Langevin equation, which implies that the autocorrelation function of $h_\alpha^*(t)$ will have an exponential form (see Appendix). In the limit where $C_3$ goes to infinity, the LCN model will revert to the LFP model with white-noise autocorrelation.

Unlike the white-noise process $\mathbf{W}(t)$, $\mathbf{h}^*(t)$ has nonzero autocorrelation times, and will be correlated with $\boldsymbol{\phi}^*(t)$. Thus, the matrix $\mathbf{D}^*$ must be chosen so that the equation for conditional scalar covariance remains unchanged. This condition yields

$$2\mathbf{D}^* = \mathbf{S}_\chi^{-1}\langle\langle\boldsymbol{\chi}|\boldsymbol{\phi}^*\rangle^*\mathbf{S}_\phi^{-1}\mathbf{h}^*\boldsymbol{\phi}'^{*\mathrm{T}}\rangle^*\mathbf{S}_\chi^{-1} + \mathbf{S}_\chi^{-1}\langle\langle\boldsymbol{\chi}|\boldsymbol{\phi}^*\rangle^*\mathbf{S}_\phi^{-1}\mathbf{h}^*\boldsymbol{\phi}'^{*\mathrm{T}}\rangle^{*\mathrm{T}}\mathbf{S}_\chi^{-1}, \tag{55}$$

where the outer-most angled brackets on the right-hand side refer to averaging with respect to the PDF of the scalars conditioned on the turbulence frequency. This expression can be further simplified for Gaussian scalars to

$$\mathbf{D}^* = \tfrac{1}{2}(\mathbf{g}^\dagger\mathbf{E}^* + \mathbf{E}^{*\mathrm{T}}\mathbf{g}^\dagger), \tag{56}$$

where $\mathbf{g}^\dagger$ is the gradient correlation matrix

$$\mathbf{E}^* \equiv \mathbf{S}_\chi\mathbf{S}_\phi^{-1}\langle\mathbf{h}^*\mathbf{v}^{*\mathrm{T}}\rangle^*\mathbf{S}_\phi\mathbf{S}_\chi^{-1}, \tag{57}$$

and $v_\alpha^* \equiv \phi_\alpha'^*/\sqrt{\langle\phi_\alpha'^2\rangle^*}$ are the standardized scalars. Note that

$$\mathbf{S}_\phi\mathbf{S}_\chi^{-1} = \mathbf{diag}\left(\sqrt{\tau_1^\dagger},\ldots,\sqrt{\tau_N^\dagger}\right), \tag{58}$$

where $\tau_\alpha^\dagger$ $(\alpha = 1,\ldots,N)$ are the scalar time scales provided by the LSR model.

For the two-scalar case, Eq. (56) yields

$$\mathbf{D}^* = \begin{bmatrix} e_{11}^* + g_{12}^\dagger e_{21}^* & \tfrac{1}{2}(e_{12}^* + e_{21}^*) + \tfrac{1}{2}g_{12}^\dagger(e_{11}^* + e_{22}^*) \\ \tfrac{1}{2}(e_{12}^* + e_{21}^*) + \tfrac{1}{2}g_{12}^\dagger(e_{11}^* + e_{22}^*) & e_{22}^* + g_{12}^\dagger e_{12}^* \end{bmatrix}, \tag{59}$$

where $e_{\alpha\beta}^*$ (for $\alpha,\beta = 1,2$) are the components of $\mathbf{E}^*$. In order to compute $\mathbf{E}^*$, the matrix

$$\langle\mathbf{h}^*\mathbf{v}^{*\mathrm{T}}\rangle^* = \begin{bmatrix} \langle h_1^* v_1^*\rangle^* & \langle h_1^* v_2^*\rangle^* \\ \langle h_2^* v_1^*\rangle^* & \langle h_2^* v_2^*\rangle^* \end{bmatrix}, \tag{60}$$

must be estimated from the notional particles. Note, however, that the expected values on the right-hand side are conditioned on the turbulence frequency. To estimate these terms, it would be necessary to divide the notional particles into subensembles, each of which having the same velocity $u^*(t)$ and turbulence frequency $\omega^*(t)$. However, computer experiments have revealed that the unconditional matrix $\langle\mathbf{h}^*\mathbf{v}^{*\mathrm{T}}\rangle$ provides a good estimate for $\langle\mathbf{h}^*\mathbf{v}^{*\mathrm{T}}\rangle^*$. Thus, since the unconditional matrix is simpler and does not require the laborious use of subensembles, we will adopt it in the remainder of this work.

The parameter $C_2$ controls the magnitude of the colored-noise term in Eq. (52), and hence affects the scalar autocorrelation function $\rho_\alpha^*(\tau)$. Computer experiments have revealed that in the two-scalar case if $C_2$ is too small [e.g., near zero as in Eq. (17)], then $\rho_\alpha^*(\tau)$ will fall to negative values before returning to zero for large $\tau$. On the other hand, if $C_2$ is too large, the scalar autocorrelation functions are always positive but fall too quickly. For the two-scalar case, the diagonal elements of the standardized matrix defined in Eq. (60) are used to fix $C_2$

$$C_2 = \frac{2}{\min(\langle h_1^* v_1^*\rangle^*, \langle h_2^* v_2^*\rangle^*)}. \tag{61}$$

For the Reynolds and Schmidt numbers of the DNS under consideration, a typical value is (see Appendix) $C_2 \approx \sqrt{2(3+C_3)} \approx 3.5$.

The parameter $C_3$ controls the autocorrelation times of $\mathbf{h}^*(t)$ and, indirectly, those of $\boldsymbol{\phi}^*(t)$. Comparisons of LCN model predictions with DNS data for the scalar autocorrelation functions have revealed that $C_3$ must vary with Reynolds number. Good agreement with DNS can be obtained with

$$C_3 = 0.692C_0, \tag{62}$$

where $C_0$ (which determines the velocity autocorrelation time) is given by Eq. (9). Unlike $C_2$, the value of $C_3$ has no effect on the velocity-scalar cross-correlation function $\rho_{u\alpha}^*(\tau)$. We thus choose $C_2$ [Eq. (61)] first to yield reasonable functional forms for $\rho_\alpha^*(\tau)$ and $\rho_{u\alpha}^*(\tau)$, and then $C_3$ [Eq. (62)] so that the scalar integral correlation times for $Sc = 1$ agree with DNS as closely as possible.

### C. Joint scalar dissipation rate

The instantaneous scalar dissipation rates are not provided by the LSR model (which gives only values conditioned on the turbulence frequency). To compare with DNS,

a stochastic model for $\chi^*_{\alpha\beta}(t)$ that is consistent with $\langle\chi_{\alpha\beta}\rangle^*(t)$ is thus necessary. Here, a simple linear model is employed using two new random variables $g_1^*(t)$ and $g_2^*(t)$

$$\mathrm{d}\begin{bmatrix} g_1^*(t) \\ g_2^*(t) \end{bmatrix} = -C_4 \begin{bmatrix} g_1^*(t) \\ g_2^*(t) \end{bmatrix} \mathrm{d}t + C_4^{1/2} \begin{bmatrix} \sqrt{1+g_{12}^\dagger(t)} & \sqrt{1-g_{12}^\dagger(t)} \\ \sqrt{1+g_{12}^\dagger(t)} & -\sqrt{1-g_{12}^\dagger(t)} \end{bmatrix} \mathrm{d}\mathbf{W}(t). \tag{63}$$

With this model, $g_1^*(t)$ and $g_2^*(t)$ are joint Gaussian random processes with

$$\langle g_1^*(t)|\boldsymbol{\epsilon}^*(s), s\leqslant t\rangle = \langle g_2^*(t)|\boldsymbol{\epsilon}^*(s), s\leqslant t\rangle = 0, \tag{64}$$

$$\langle g_1^*(t)g_1^*(t)|\boldsymbol{\epsilon}^*(s), s\leqslant t\rangle = \langle g_2^*(t)g_2^*(t)|\boldsymbol{\epsilon}^*(s), s\leqslant t\rangle = 1, \tag{65}$$

and

$$\langle g_1^*(t)g_2^*(t)|\boldsymbol{\epsilon}^*(s), s\leqslant t\rangle = g_{12}^\dagger(t). \tag{66}$$

The model can be extended to more than two scalars by using the scalar-gradient correlation matrix $\mathbf{g}^\dagger(t) \equiv [g_{\alpha\beta}^\dagger(t)]$. The case of perfectly correlated scalars where $\mathbf{g}^\dagger(t)$ is rank-deficient can be handled using the eigenvalue decomposition described above for the LFP model. For the two-scalar case, $g_{12}^\dagger(t)=1$ implies that $g_1^*(t)=g_2^*(t)$, so that the eigenvalue decomposition is not required.

The parameter $C_4$ is inversely proportional to the autocorrelation times of $g_1^*(t)$ and $g_2^*(t)$. In this work, the Reynolds-number dependence is fit to DNS data[10] for $\chi^+(t)$ with $Sc=1$

$$C_4 = 0.346 Re_1^{0.695}. \tag{67}$$

Note that (according to this model) $g_1^*(t)$ and $g_2^*(t)$ have identical autocorrelation times. This is justified by the fact that in the LSR model the characteristic frequency for the joint scalar dissipation (denoted by $\delta_{\alpha\beta}\langle r_{\alpha\beta}\rangle_D^\dagger$ in earlier work[4]) is independent of Schmidt number. Likewise, in DNS the autocorrelations of dissipation rates of different scalars are almost identical. Moreover, for very large Reynolds numbers, the autocorrelation times approach zero. In this limit, $g_1^*(t)$ and $g_2^*(t)$ can be represented by joint-Gaussian white-noise processes.

The scalar dissipation rates are found from $g_1^*(t)$ and $g_2^*(t)$ using the following model:

$$\chi_1^*(t) = g_1^*(t)g_1^*(t)\langle\chi_1\rangle^*(t), \tag{68}$$

$$\chi_2^*(t) = g_2^*(t)g_2^*(t)\langle\chi_2\rangle^*(t), \tag{69}$$

and

$$\chi_{12}^*(t) = g_1^*(t)g_2^*(t)\sqrt{\langle\chi_1\rangle^*(t)\langle\chi_2\rangle^*(t)}. \tag{70}$$

Note that expected values of $\chi_{\alpha\beta}^*(t)$ as defined above yield the desired results. For example,

$$\begin{aligned}\langle\chi_1^*(t)\rangle &= \langle\langle[g_1^*(t)g_1^*(t)\langle\chi_1\rangle^*(t)]|\boldsymbol{\epsilon}^*(s), s\leqslant t\rangle\rangle \\ &= \langle\langle g_1^*(t)g_1^*(t)|\boldsymbol{\epsilon}^*(s), s\leqslant t\rangle\langle\chi_1\rangle^*(t)\rangle \\ &= \langle\langle\chi_1\rangle^*(t)\rangle = \langle\chi_1\rangle,\end{aligned} \tag{71}$$

where the outer-most angled brackets on the right-hand side refer to averages with respect to the conditioning variable $\{\boldsymbol{\epsilon}^*(s), s\leqslant t\}$. Also note that the correlation time of $\chi_\alpha^*(t)$ depends on $Sc$ only via $\langle\chi_\alpha\rangle^*(t)$, which is obtained from the LSR model.

From the definitions given above [Eqs. (68)–(70)], it follows that the fluctuating gradient vectors of different scalars are assumed to be perfectly aligned:

$$\nabla\phi_\alpha(\mathbf{X}^*(t),t) = g_\alpha^*(t)\left(\frac{\langle\chi_\alpha\rangle^*(t)}{D_\alpha}\right)^{1/2}\mathbf{n}(\mathbf{X}^*(t),t), \tag{72}$$

where $\mathbf{n}(\mathbf{x},t)$ is a unit vector which is randomly oriented but the same for all the scalars involved. Strictly speaking, this would only occur if the scalar fields were one-dimensional (as in the linear-eddy and one-dimensional turbulence models of Kerstein[32,33]). However, it should also be a reasonable assumption for the present case where the mean scalar gradients are perfectly aligned. In the limit where $Sc_1=Sc_2$, the scalar-gradient fields will be identical since $g_1^*(t)=g_2^*(t)$. Another interesting limiting case is that of nonturbulent flow wherein $\langle\chi_\alpha\rangle^*(t)$ is a deterministic function of time,[31] for which the one-dimensional scalar-gradient field will be Gaussian[31] as predicted by the model for $g_\alpha^*(t)$.

In terms of the model described above for estimating $\langle\chi_\alpha^*(t)|\boldsymbol{\epsilon}^*(s), s\leqslant t\rangle$ over a sphere of diameter $L_\epsilon$, the random variables $g_\alpha^*(t)$ would represent scalar-gradient fluctuations within the sphere. The scalar-gradient field is thus assumed to be *locally* Gaussian, but globally non-Gaussian due to the random variable $\langle\chi_\alpha\rangle^*(t)$. In turbulent flow, the latter can vary significantly from its mean value[13] $\langle\chi_\alpha\rangle$, leading to large deviations from Gaussianity.

The PDF of the scalar dissipation rate defined by Eq. (68) will depend on the joint PDF of $g_1^*$ and $\langle\chi_1\rangle^*$. However, from the model for $g_1^*(t)$ [Eq. (63)], we can note that these variables should be nearly independent. In addition, because $g_1^*$ will be Gaussian, its square appearing in Eq. (68) will have a chi-squared PDF with one degree of freedom so that $\langle(g_1^*)^2\rangle=1$ and $\langle(g_1^*)^4\rangle=3$. The variance of $\chi_1^*(t)$ can thus be expressed as

$$\sigma^2(\chi_1) = \langle\chi_1\rangle^2(3\beta-1), \tag{73}$$

where

$$\beta = \frac{\langle(\langle\chi_1\rangle^*)^2\rangle}{\langle\chi_1\rangle^2} \geqslant 1, \tag{74}$$

is a measure of the correlation between $\langle\chi_1\rangle^*$ and $\omega^*$. The latter can be quantified using the conditional expectation

TABLE III. Statistical measures of the energy dissipation rate. The symbols $\mu(\cdot)$, $\sigma(\cdot)$, $\sigma^2(\cdot)$, $\mu_3(\cdot)$, and $\mu_4(\cdot)$ denote the mean, rms, variance, skewness and flatness, respectively, of the bracketed quantities.

| | 38 | | 91 | | 134 | | 234 | |
|---|---|---|---|---|---|---|---|---|
| $R_\lambda$ | DNS | Model | DNS | Model | DNS | Model | DNS | Model |
| $\sigma(\epsilon)/\mu(\epsilon)$ | 0.97 | 0.97 | 1.15 | 1.13 | 1.24 | 1.21 | 1.46 | 1.36 |
| $\mu_3(\epsilon)$ | 2.86 | 2.92 | 4.08 | 3.94 | 4.49 | 4.61 | 6.31 | 6.27 |
| $\mu_4(\epsilon)$ | 19 | 20 | 37 | 37 | 44 | 55 | 114 | 135 |
| $\sigma^2(\ln \epsilon)$ | 0.81 | 0.87 | 0.97 | 1.04 | 1.07 | 1.13 | 1.25 | 1.27 |
| $\mu_3(\ln \epsilon)$ | −0.25 | −0.42 | −0.18 | −0.35 | −0.15 | −0.33 | −0.09 | −0.30 |
| $\mu_4(\ln \epsilon)$ | 3.23 | 3.47 | 3.16 | 3.39 | 3.09 | 3.37 | 3.07 | 3.35 |

$\langle \chi_1 | \epsilon \rangle$, by setting $\beta = \langle \langle \chi_1 | \epsilon \rangle^2 \rangle / \langle \chi_1 \rangle^2$. In Vedula *et al.*,[13] the functional form of $\langle \chi | \epsilon \rangle / \langle \chi \rangle$ was found to be nearly independent of both Reynolds and Schmidt numbers. In the LSR model, the functional form is determined by the stretching exponent in Eq. (24) and turbulent frequency autocorrelation time constant $C_1$ in Eq. (10). As discussed in Sec. IV, comparison of model predictions with DNS data suggests that $\gamma = 1$ yields better agreement than $\gamma = 0.5$ and that, contrary to Eq. (13), $C_1$ must be independent of Reynolds number.

## IV. DNS VALIDATION RESULTS

In this section we present model results in comparison with DNS, first via single-point Eulerian statistics (Secs. IV A–IV C) used to validate model assumptions, and then via Lagrangian statistics (Secs. IV D–IV F) used to evaluate the ultimate model performance. Reynolds number dependence is considered in the tables and first few figures. However, for the sake of brevity, Lagrangian results in graphical form are given for the case of the highest Reynolds number only.

### A. Moments and PDF of energy dissipation

Because the DNS data and model predictions are for statistically homogeneous flow, Eulerian statistics can be estimated directly from the Lagrangian data via ensemble averages. Eulerian statistics for the energy dissipation and its logarithm predicted by Eq. (10) are presented in Table III, along with the corresponding values from DNS.[13] Excellent agreement for the moments of $\epsilon$ is obtained, which is a result of fitting $\gamma_1$ [see Eq. (11)] to the DNS data. Note that as the Reynolds number increases, the flatness factor $\mu_4(\epsilon)$ increases significantly, reflecting a higher degree of intermittency.

The standardized PDF of $\ln \epsilon$ is shown in Fig. 1, where it can be seen that the agreement between the model and DNS is excellent. Note that this PDF appears to be slowly approaching a log-normal distribution with increasing Reynolds number, with (as suggested by results in Table III where the skewness and flatness of $\ln \epsilon$ approach 0 and 3, respectively) the model approaching slightly more slowly than the DNS.

### B. Moments and PDF of scalar dissipation

Eulerian statistics for the scalar dissipation rate predicted by the model are presented in Table IV. As noted earlier, the value of $r_\phi$ for $Sc = 1$ has been fit to the DNS data at each Reynolds number. However, because of correlation between the energy and scalar dissipation in Eq. (23), the model does not reproduce the DNS values exactly. Indeed, if $\omega^*$ and $\langle \chi_\alpha \rangle^*$ in Eq. (23) were uncorrelated,[27] then $r_\phi$ predicted by the LSR model would agree exactly with DNS. On the other hand, the value of $r_\phi$ at other Schmidt numbers is predicted by the model. In general, the agreement is satisfactory given the simple description of spectral transfer provided by the LSR model, and the fact that in DNS volume-averaged statistics such as the mean values of the scalar dissipation can vary substantially in time.

Moments of $\chi$ from DNS shown in Table IV increase both with Reynolds number and Schmidt number. However, the model predictions are essentially independent of Reynolds and Schmidt numbers. As noted after Eq. (73), the moments predicted by the model depend on $g^*$ for each

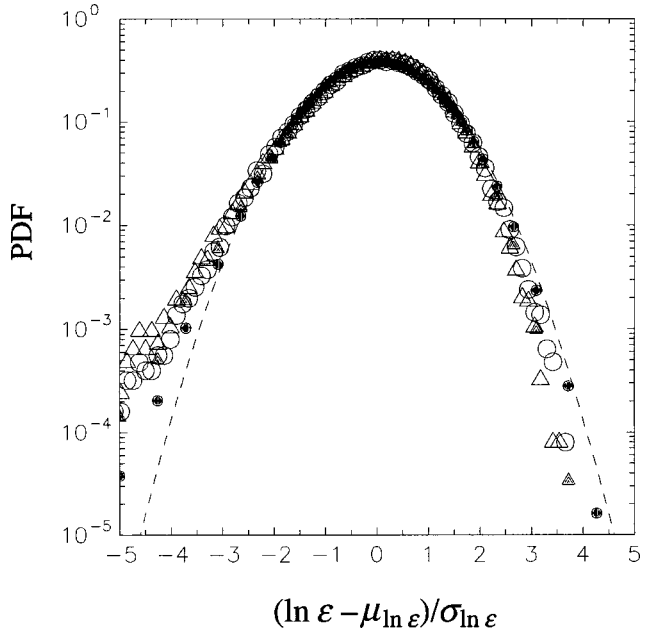


FIG. 1. Standardized PDFs of $\ln \epsilon$ from LSR model compared with DNS at $R_\lambda$ 38 (triangles) and 234 (circles). Filled symbols: DNS. Open symbols: Model. Dashed curve represents a standard Gaussian distribution.

TABLE IV. Statistical moments involving the scalar dissipation rate.

| | 38 | | | | 91 | | | |
|---|---|---|---|---|---|---|---|---|
| | 1/4 | | 1 | | 1/8 | | 1 | |
| $R_\lambda$ / $Sc$ | DNS | Model | DNS | Model | DNS | Model | DNS | Model |
| $r_\phi$ | 2.83 | 2.26 | 1.84 | 1.82 | 3.74 | 3.16 | 2.55 | 2.37 |
| $\sigma(\chi)/\mu(\chi)$ | 1.73 | 1.78 | 2.14 | 1.80 | 2.00 | 1.80 | 2.62 | 1.81 |
| $\mu_3(\chi)$ | 4.85 | 5.63 | 6.28 | 5.83 | 5.39 | 5.71 | 7.76 | 5.73 |
| $\mu_4(\chi)$ | 42 | 70 | 72 | 77 | 52 | 74 | 112 | 74 |
| $\sigma^2(\ln\chi)$ | 1.86 | 5.13 | 2.59 | 5.14 | 2.13 | 5.17 | 3.22 | 5.17 |
| $\mu_3(\ln\chi)$ | −0.174 | −1.35 | −0.115 | −1.34 | −0.113 | −1.35 | −0.098 | −1.33 |
| $\mu_4(\ln\chi)$ | 3.13 | 5.95 | 2.87 | 5.87 | 3.05 | 5.97 | 2.82 | 5.89 |
| | 134 | | | | 234 | | | |
| | 1/8 | | 1 | | 1/8 | | 1 | |
| $R_\lambda$ / $Sc$ | DNS | Model | DNS | Model | DNS | Model | DNS | Model |
| $r_\phi$ | 3.19 | 2.78 | 2.45 | 2.27 | 2.75 | 2.64 | 2.38 | 2.17 |
| $\sigma(\chi)/\mu(\chi)$ | 2.27 | 1.80 | 2.62 | 1.81 | 3.01 | 1.79 | 3.22 | 1.79 |
| $\mu_3(\chi)$ | 6.64 | 5.65 | 7.56 | 5.68 | 9.90 | 5.45 | 10.41 | 5.45 |
| $\mu_4(\chi)$ | 78 | 72 | 103 | 73 | 182 | 66 | 241 | 66 |
| $\sigma^2(\ln\chi)$ | 2.60 | 5.18 | 3.31 | 5.17 | 3.37 | 5.18 | 3.73 | 5.17 |
| $\mu_3(\ln\chi)$ | −0.065 | −1.34 | −0.055 | −1.33 | −0.018 | −1.34 | −0.012 | −1.33 |
| $\mu_4(\ln\chi)$ | 2.88 | 5.92 | 2.81 | 5.88 | 2.82 | 5.91 | 2.82 | 5.85 |

scalar [see Eq. (63)] and the conditional dissipations $\langle\chi|\epsilon\rangle$, which are statistically independent of each other. From DNS, the functional form of $\langle\chi|\epsilon\rangle$ is (see Fig. 8 in Ref. 11) nearly independent of Reynolds and Schmidt number; judging from Fig. 3, this feature is adequately predicted by the LSR model. As a result, any Reynolds and Schmidt number dependence appearing in Table IV must come from $g^*$ and $\epsilon$. Since the latter can only depend on Reynolds number, any Schmidt number dependence can only be accounted for via the model for $g^*$. Thus, the mismatch between model predictions and DNS points to the need for a more sophisticated model for $g^*$.

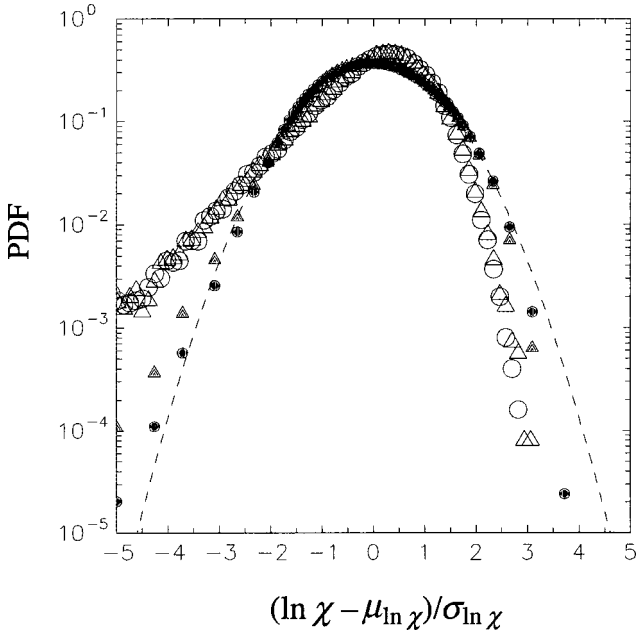


FIG. 2. Standardized PDFs of $\ln\chi$ from LSR model compared with DNS at $R_\lambda$ 38, $Sc=1$ (triangles) and $R_\lambda$ 234, $Sc=1$ (circles). Filled symbols: DNS. Open symbols: Model. Dashed curve represents a standard Gaussian distribution.

The moments of $\ln\chi$ are also presented in Table IV, while the PDF is shown in Fig. 2. In general, the model PDF is more skewed to negative values than in DNS. This can mainly be attributed to the fact that $g^*$ is normally distributed, and thus the PDF of $(g^*)^2$ is a chi-squared distribution with one degree of freedom. In order to improve the agreement, Eq. (63) would need to be replaced by a more complicated nonlinear model with the same means and covariances. Yet, because $\chi^*$ is not needed in the LFP and LCN models (only $\langle\chi\rangle^*$ is required), there is little motivation to attempt to improve the model for $g^*$ at present.

### C. Conditional statistics

Statistical properties conditioned on the energy dissipation rate play a prominent role in the LSR model. In earlier work,[13] DNS data was used to conduct *a priori* testing of various modeled terms in the Eulerian equations for the energy-dissipation-conditioned scalar variance and scalar dissipation rate. It is thus of interest to extract conditional statistics predicted by the modified LSR model for *a posteriori* validation with DNS. In particular, we are interested in the normalized conditional scalar dissipation rate $\langle\chi|Z\rangle/\langle\chi\rangle$, and the normalized conditional scalar variance $\langle\phi'^2|Z\rangle/\langle\phi'^2\rangle$, where

$$Z=\frac{\ln\epsilon-\mu_{\ln\epsilon}}{\sigma_{\ln\epsilon}}. \tag{75}$$

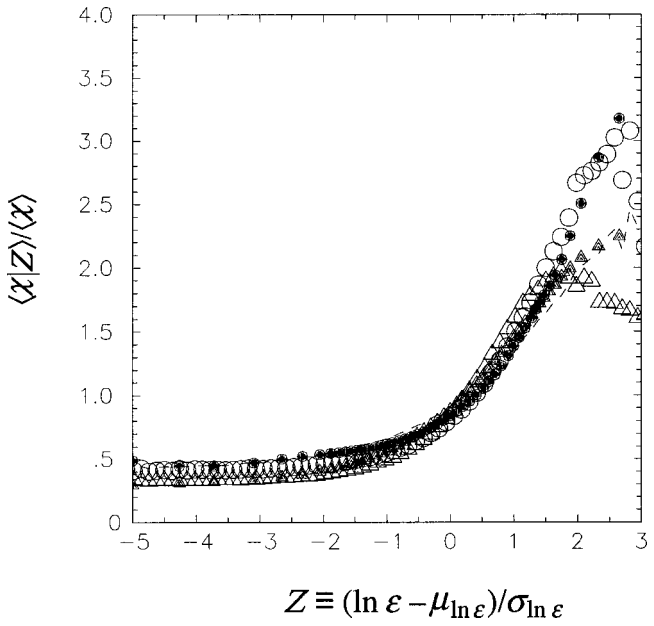


FIG. 3. Normalized conditional scalar dissipation rate as function of energy dissipation for $R_\lambda$ 38, $Sc=1$ (circles) and $R_\lambda$ 234, $Sc=1$ (triangles). Filled symbols: DNS. Open symbols: Model ($\gamma=1$). Dashed curve is model prediction for $R_\lambda$ 38 and $Sc=1$ with $\gamma=0.5$.

In DNS (see Vedula *et al.*[13]) both of these were found to be nearly independent of the Reynolds and Schmidt numbers.

Model comparisons for these two conditional quantities are shown in Figs. 3 and 4, respectively. It is apparent that the differences between results at $R_\lambda$ 38 and 234 for large $Z$ are much stronger in the model than in DNS. As discussed by Fox,[3] this difference can be traced to the increase of $C_1$ [Eqs. (10) and (13)] with Reynolds number. The effect of the stretching exponent $\gamma$ [Eq. (24)] has been tested using two values ($\gamma=0.5$ and 1). It can be seen that although larger values of $\gamma$ improve the agreement, $\gamma=1$ is not sufficient to overcome the decrease in correlation caused by the smaller autocorrelation time for $\omega^*$. This difference may be due partly to the fact that a white-noise model is being used for $\omega^*$, which results in rapid fluctuations in $\sigma^*$. If a colored-noise model were used for $\omega^*$, the correlation between $\sigma^*$ and $\chi^*$ generated by the gradient amplification term would perhaps be stronger. Nevertheless, we can conclude that in order for $\langle\chi|Z\rangle/\langle\chi\rangle$ and $\langle\phi'^2|Z\rangle/\langle\phi'^2\rangle$ to be (as seen in DNS) nearly independent of $R_\lambda$ and $Sc$, $C_1$ must be made independent of Reynolds number.

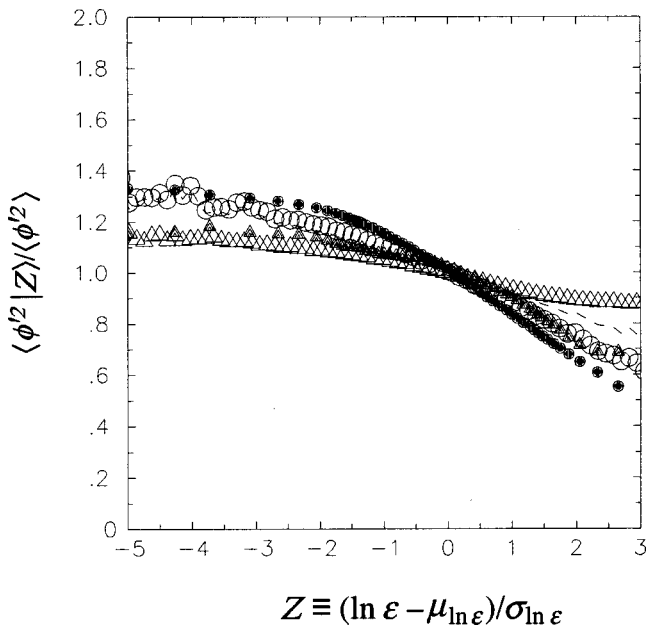


FIG. 4. Normalized conditional scalar variance for same conditions as in Fig. 3.

In our earlier work,[4] the combination $C_1=5$, $\gamma=0.5$ and $C_s=1$ [Eq. (23)] were found to yield good agreement with DNS. Dreeben and Pope[34] were the first to propose $C_1=5$ (denoted $C_3$ in their work), albeit based on other physical constraints. However, use of this value would cause the autocorrelation time of $\omega^*$ to disagree with the autocorrelation time from DNS. Depending on the application, it may thus be necessary to distinguish between the scalar-gradient amplification forcing function $\sigma^*(t)$ and the turbulence frequency $\omega^*(t)$. When $\gamma=1$, both would be governed by the same stochastic differential equation (and thus have the same PDF), but the coefficients for $\sigma^*(t)$ would be independent of Reynolds number.

Finally, note that because the conditional scalar variance is a random variable, the scalar PDFs predicted by the model have higher order moments that are slightly larger than Gaussian.[3] Representative values for scalar flatness and superskewness are 3.03 and 15.5, respectively, compared to 3 and 15 for Gaussian random variables. As discussed above, if $C_1$ is held constant so that $\langle\phi'^2|Z\rangle/\langle\phi'^2\rangle$ is independent of Reynolds and Schmidt number, then the scalar flatness and superskewness would also be independent of $R_\lambda$ and $Sc$.

### D. Typical Lagrangian time series

Typical time series for $R_\lambda$ 234 found from DNS, the LFP model, and the LCN model are shown in Figs. 5–7, respectively. The time axis in each figure is scaled by the velocity integral time scale $T_L$. Looking first at the velocity, it can be seen that the DNS time series is ''smoother'' on short time scales than the model. This behavior is a result of using a Langevin white-noise model for velocity. Looking next at the scalars, the LFP model also exhibits short time scale fluctuations characteristic of a Langevin white-noise process. In contrast, the time series from DNS and the LCN model are clearly much smoother. The lack of smoothness in the LFP time series does not necessarily imply a significant difference in autocorrelation times; however, it is reflected in the shapes of the autocorrelation functions and other measures of short-time behavior. Finally, note that even though the dissipation rates of different scalars are significantly correlated, it is still possible that they attain high values at different time instants.

### E. Autocorrelation functions

The most important statistical quantities characterizing Lagrangian time series such as those illustrated above are the autocorrelations as a function of time lag, which we have obtained using the same methods as used for DNS data in

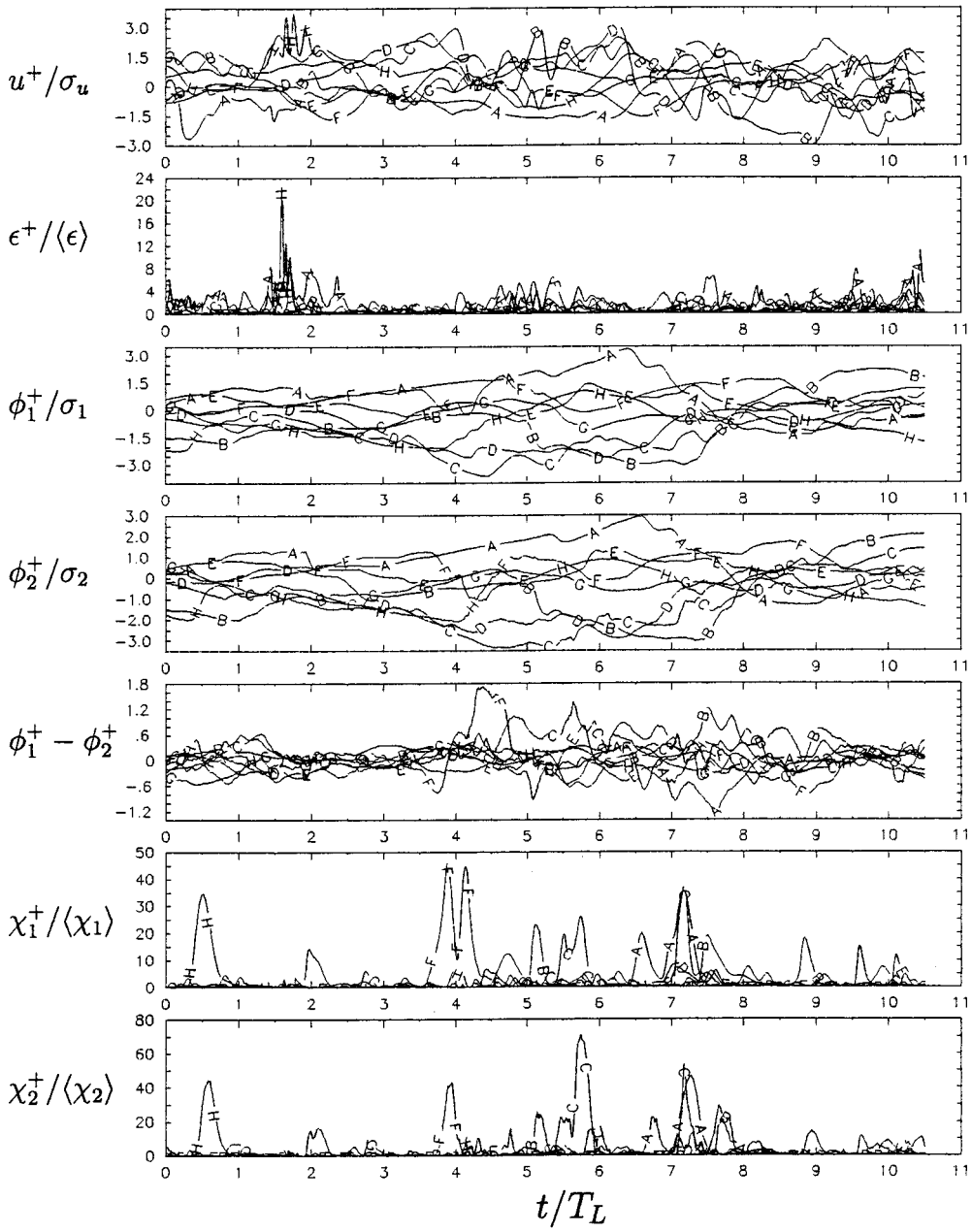


FIG. 5. (Same as Fig. 1 in Ref. 10.) Typical Lagrangian time series of normalized Lagrangian quantities from $512^3$ simulation, from top to bottom: (i) velocity, (ii) energy dissipation, (iii) scalar $\phi_1$ with $Sc=1/8$, (iv) scalar $\phi_2$ with $Sc=1$, (v) difference $\phi_1-\phi_2$, (vi) dissipation of $\phi_1$, and (vii) dissipation of $\phi_2$. Each data line (A to H) represents a different fluid particle in the sample.

Ref. 10. These autocorrelation functions are, in turn, characterized by both their shapes and their integral time scales, which give a rough measure of the memory time associated with each variable. Correlation functions for a closely related linear constant-coefficient model are derived in the Appendix. The integral time scales are reported in Table V, where it can be seen that the velocity and energy dissipation are well predicted by the model. This is not surprising, since the model parameters that control the autocorrelation times were fit to DNS. [Recall, however, that via the choice of Eq. (13) this is achieved at the expense of agreement for the conditional statistics presented in Sec. IV C.] The same can be said for the scalar dissipation rates since $C_4$ in Eq. (63) was fit to DNS data for $Sc=1$. It is noteworthy that both models (LFP and LCN) predict the correct dependence of $T_\phi$ and $T_\chi$ on Schmidt number. This fact is mainly due to the Schmidt number dependence of the LSR model predictions for $r_\phi$.

More interesting are the model values for the autocorrelation times of the scalar fluctuations. From Table V, it can be seen that the LCN model yields reasonably good predictions at every Reynolds number, while the LFP model underpredicts. For the LFP model, the autocorrelation function depends on $r_\phi$, $C_2$ and $C_0$, none of which can be adjusted to improve the predictions. On the other hand, the LCN model has an additional parameter $C_3$ that can be used to control the scalar autocorrelation time for $\phi_2$ $(Sc=1)$. In

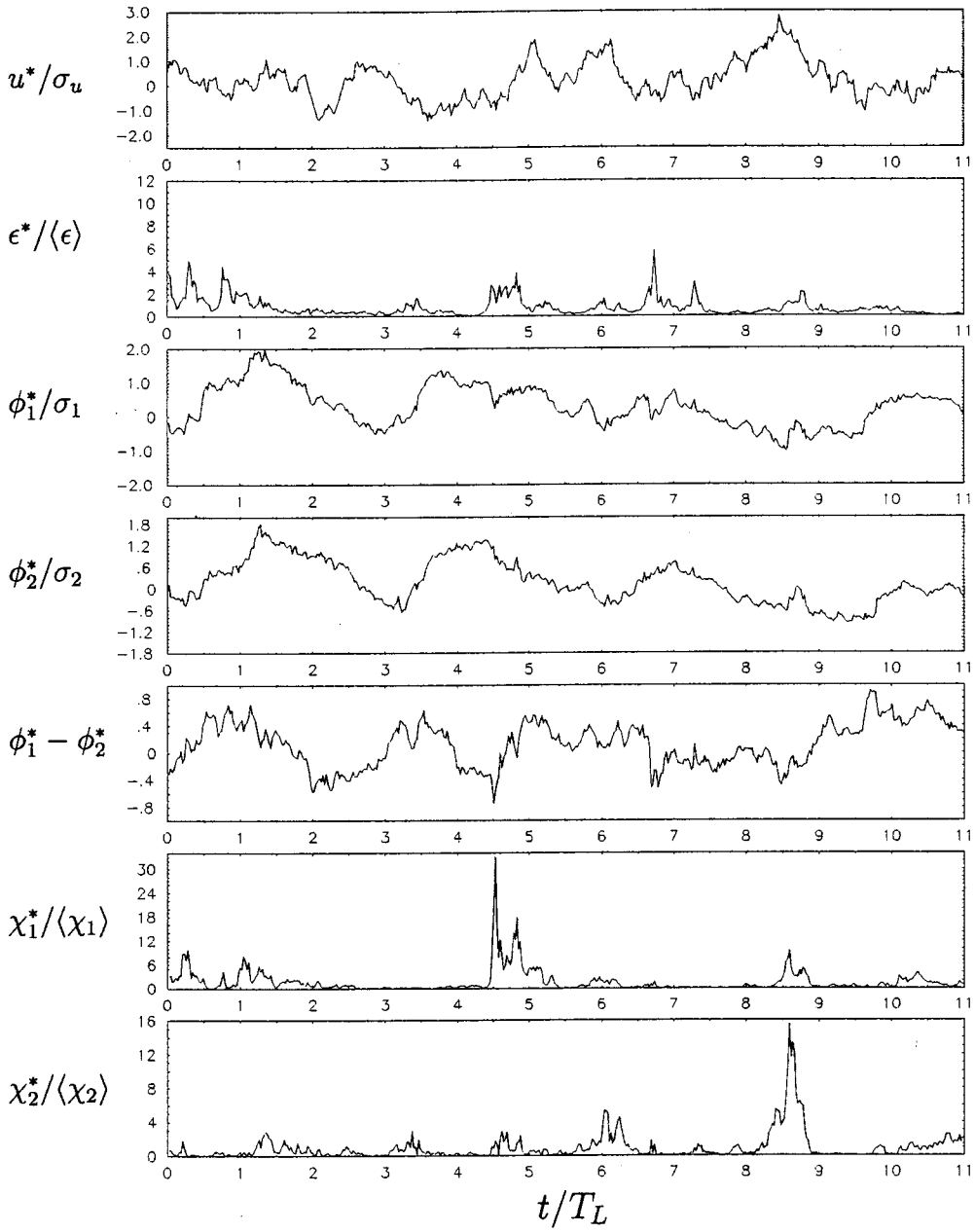


FIG. 6. Typical Lagrangian time series from the LFP model for the same conditions as in Fig. 5. For brevity, just one sample is shown for each quantity.

this work, we have used Eq. (62) to fit $C_3$; however, there is no firm physical justification for this choice, especially at low Reynolds numbers. In particular, in the limit of $R_\lambda$ reaching zero, because $C_0$ in Eq. (9) becomes zero, Eq. (62) gives $C_3=0$, which is contrary to the expectation that $C_3$ should remain positive.

Although the autocorrelation times give a good indication of the accuracy of the model, the overall functional forms of the autocorrelation function provide more reliable tests of performance. The autocorrelation functions from DNS for $R_\lambda$ 234 are shown in Fig. 8. The corresponding functions predicted by the LFP and LCN models are given in Figs. 9 and 10, respectively. As noted by Yeung,[10] because the velocity and scalars are differentiable in time, the autocorrelation functions found from the Navier–Stokes and scalar transport equations will all have zero slope at the origin ($\tau=0$). (The insets in Figs. 8–10 illustrate the behavior of the energy and scalar dissipation autocorrelations at very small time lags. Note that the LFP and LCN models do not affect the scalar dissipation autocorrelation functions.) In contrast, the white-noise models [e.g., Eqs. (7), (10), and (63)] predict finite (negative) slopes. In terms of the time series, a nonzero slope yields ''noisier'' time series (compare the scalar time series in Figs. 6 and 7). It also implies a zero value for the Taylor time scale (considered elsewhere[19,35]) corresponding to an infinite value for the Lagrangian time derivative.

At high Reynolds numbers, the autocorrelation functions for the velocity, energy dissipation, and scalar dissipation rates fall off quickly and the model predictions are in good agreement with DNS. The DNS scalar autocorrelation func-

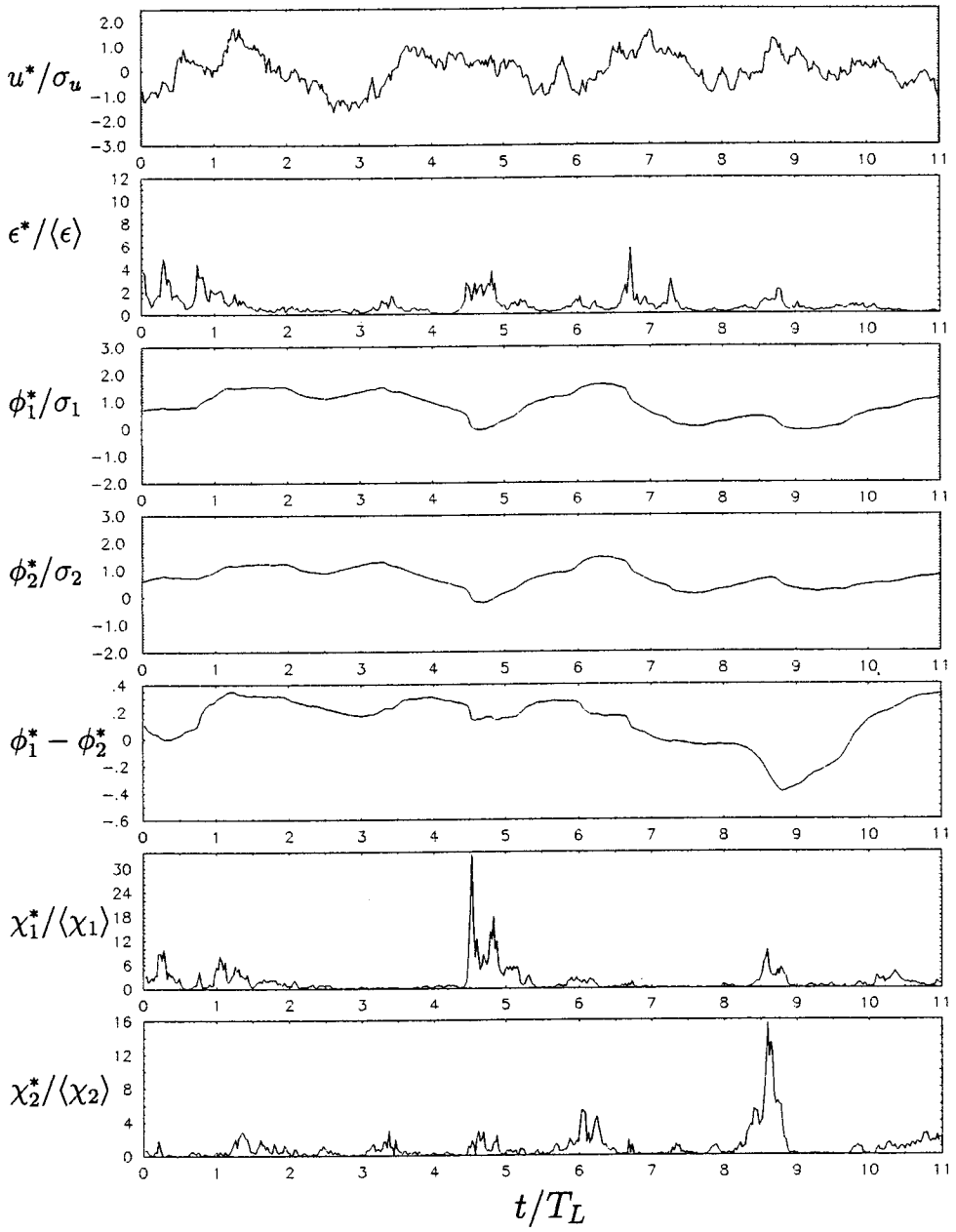


FIG. 7. Typical Lagrangian time series from the LCN model for the same conditions as in Fig. 5. For brevity, just one sample is shown for each quantity.

tions, on the other hand, fall much more slowly with a distinct zero slope at the origin at all Reynolds numbers. In contrast to the LFP model, the LCN model closely reproduces the DNS autocorrelation functions at all Reynolds numbers. Based on these observations, we conclude that the LCN model yields the more realistic Lagrangian scalar time series.

### F. Cross-correlation functions

Correlation coefficients between the velocity and scalars are presented in Table VI for DNS and both scalar mixing models. The model predictions for the scalar correlation coefficients are near unity, and follow the trends seen in earlier work.[4] For the LFP model, the predicted velocity-scalar correlation coefficient is approximately

$$\rho_{u\phi} \approx -\left[\frac{r_\phi}{(1+C_2)r_\phi + 3C_0/2}\right]^{1/2}. \tag{76}$$

(As shown in the Appendix, this expression would be exact if the coefficient matrices $\mathbf{M}^*$ and $\mathbf{B}^*$ were constants.) Given that the value of $C_0$ is fixed by the velocity model, the velocity-scalar correlation coefficients predicted by the mixing models can never be as large as the DNS values (i.e., even with $C_2 = 0$). This mismatch can also be seen from the velocity-scalar cross-correlation functions shown in Figs. 11–13. In general, the models predict the correct shape (including a mild $Sc$ dependence), but not the correct magnitude as compared to DNS. The agreement with DNS is worse

TABLE V. Lagrangian autocorrelation times.

| | 38 | | | 91 | | |
|---|---|---|---|---|---|---|
| $R_\lambda$ | DNS | LFP | LCN | DNS | LFP | LCN |
| $\langle\epsilon\rangle T_u/k$ | 0.379 | 0.381 | 0.383 | 0.266 | 0.247 | 0.252 |
| $T_\epsilon/T_u$ | 0.497 | 0.396 | 0.395 | 0.411 | 0.426 | 0.417 |
| $T_{\phi 1}/T_u$ | 1.88 | 1.41 | 2.07 | 2.01 | 1.56 | 1.78 |
| $T_{\phi 2}/T_u$ | 2.17 | 1.49 | 2.27 | 2.24 | 1.71 | 2.06 |
| $T_{\chi 1}/T_u$ | 0.460 | 0.423 | 0.423 | 0.359 | 0.353 | 0.346 |
| $T_{\chi 2}/T_u$ | 0.497 | 0.406 | 0.404 | 0.333 | 0.340 | 0.333 |
| | 134 | | | 234 | | |
| $R_\lambda$ | DNS | LFP | LCN | DNS | LFP | LCN |
| $\langle\epsilon\rangle T_u/k$ | 0.245 | 0.231 | 0.234 | 0.219 | 0.219 | 0.218 |
| $T_\epsilon/T_u$ | 0.361 | 0.365 | 0.361 | 0.296 | 0.301 | 0.302 |
| $T_{\phi 1}/T_u$ | 1.73 | 1.67 | 1.97 | 2.22 | 1.86 | 2.22 |
| $T_{\phi 2}/T_u$ | 1.88 | 1.84 | 2.27 | 2.32 | 1.97 | 2.38 |
| $T_{\chi 1}/T_u$ | 0.299 | 0.299 | 0.296 | 0.227 | 0.226 | 0.227 |
| $T_{\chi 2}/T_u$ | 0.280 | 0.289 | 0.286 | 0.207 | 0.216 | 0.217 |

with the LCN model because the scalar time series varies more slowly with time (see Fig. 7), making it less correlated with the rapidly fluctuating velocity.

One way to improve the agreement with DNS would be to use a more sophisticated model for the velocity (e.g., a Langevin model for the acceleration, instead of for the velocity). Such models have been proposed by Sawford[36] and Pope,[37] but have not been investigated in conjunction with Lagrangian scalar mixing models. Because the value of $\rho_{u\phi}$ has a direct effect on the scalar variance predicted by the models, it is likely that improving the velocity model will have a significant impact on the performance of the Lagrangian PDF models for scalar transport.

Another way to improve the agreement with DNS would be to use smaller values for $C_2$ in the mixing models [Eqs. (37) and (52)]. However, numerical experiments with both mixing models have revealed that the correlation functions exhibit damped oscillations when $C_2$ is decreased. This behavior is most likely due to the unsymmetric matrix $\mathbf{S}_D\boldsymbol{\chi}^*\mathbf{S}_D^{-1}$ appearing in both mixing models. [Recall that this matrix was used in order to produce agreement with the lin-

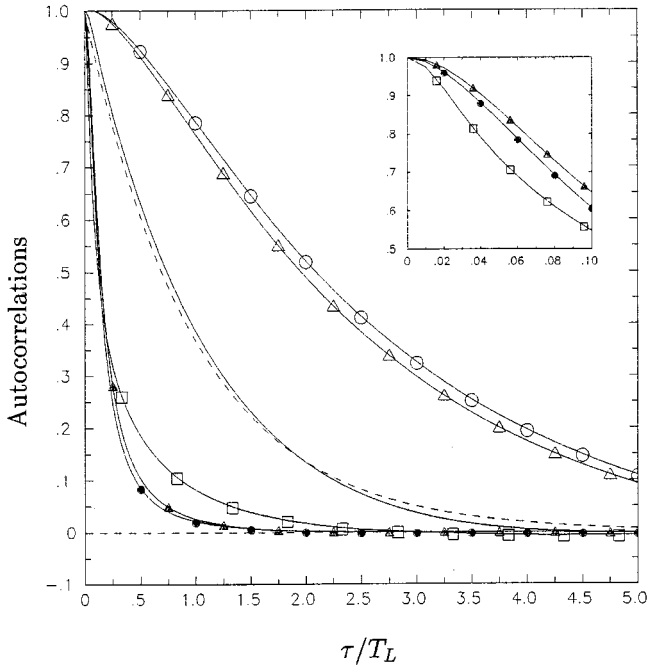


FIG. 8. (Same as Fig. 10 in Ref. 10.) Lagrangian autocorrelations from $512^3$ simulation: Velocity (unmarked solid line), energy dissipation (□), scalar $\phi_1$ at $Sc=1/8$ (△), scalar $\phi_2$ at $Sc=1$ (○), dissipation of $\phi_1$ (▲), and dissipation of $\phi_2$ (●). The dashed curve shows exponential approximation to the velocity autocorrelation. Energy and scalar dissipation autocorrelations at very small time lags ($\tau/T_u \leqslant 0.1$) are shown magnified in the inset.

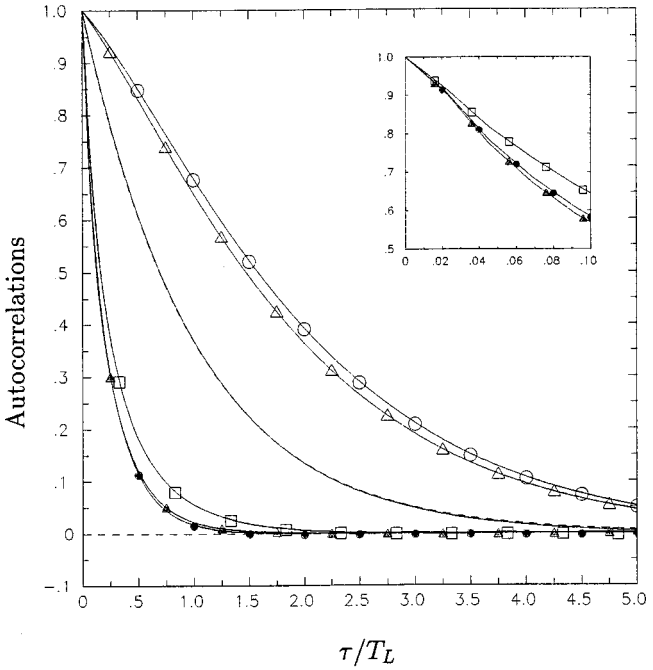


FIG. 9. Lagrangian autocorrelation functions from the LFP model for the same conditions as in Fig. 8. Note that the energy and scalar dissipation autocorrelations for the LFP and LCN models (Fig. 10) are identical.

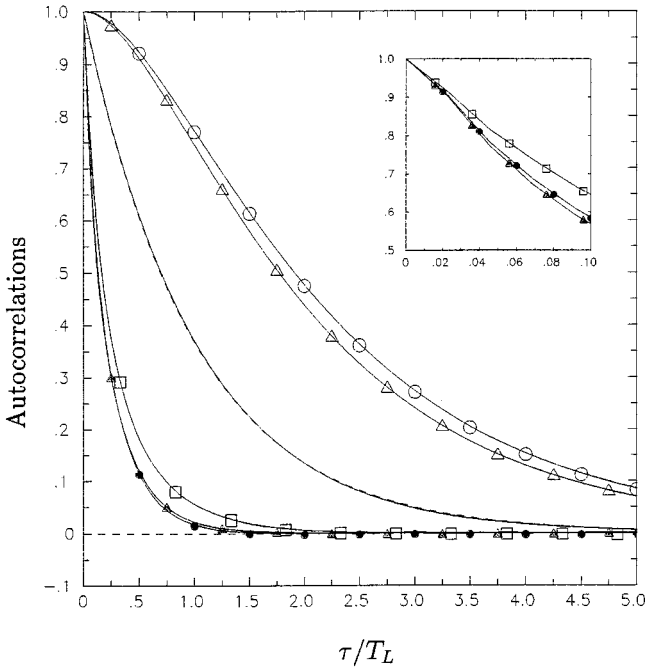


FIG. 10. Lagrangian autocorrelation functions from the LCN model for the same conditions as in Fig. 8. Note that the energy and scalar dissipation autocorrelations for the LFP (Fig. 9) and LCN models are identical.

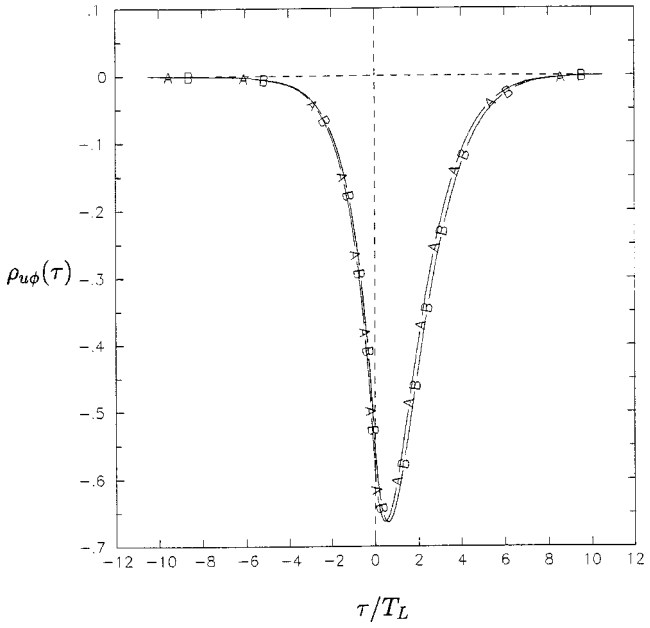


FIG. 11. (Same as Fig. 7 in Ref. 10.) Lagrangian velocity-scalar cross-correlation function, taken from $512^3$ simulation, for scalars at $Sc=1/8$ (A) and $Sc=1$ (B).

ear model [Eq. (17)] in the limit where $C_2=0$.] If this matrix were replaced with a symmetric form, i.e.,

$$\tfrac{1}{2}(\mathbf{S}_D\boldsymbol{\chi}^*\mathbf{S}_D^{-1}+\mathbf{S}_D^{-1}\boldsymbol{\chi}^*\mathbf{S}_D), \tag{77}$$

it might be possible to use smaller values of $C_2$ without observing damped oscillations in the correlation functions. However, the mixing models would no longer agree with Eq. (17) in the limit $C_2=0$.

In addition to the difficulty in capturing $\rho_{u\phi}$, we have also found that neither mixing model predicts the Reynolds-number dependence of the autocorrelation function of the scalar difference $\phi_1'^*-\phi_2'^*$ reported by Yeung.[10] Taken to gether, these observations suggest that a more sophisticated multiscale mixing model may be required to accurately reproduce DNS autocorrelation functions involving the scalars. For example, such a model could be based on the ''spectral decomposition'' used in the LSR model (i.e., by introducing random variables for each wavenumber band). In a multiscale model, scalar fluctuations generated by $u^*$ in Eq. (15) would dominate in the low wavenumber range, while $\langle \mathbf{D}\nabla^2\boldsymbol{\phi}'|\boldsymbol{\phi}^*\rangle^*$ would affect only the scalar-dissipation range. At high Reynolds numbers, this would lead to a ''natural'' separation of scales, which would result in higher values for $\rho_{u\phi}$ and ''smoother'' scalar time series (without resorting to a colored-noise mixing model). We plan to explore the use of multiscale mixing models in a future communication that focuses on two-scalar Lagrangian statistics.

Finally, examples of the energy-scalar dissipation cross-correlation function are shown in Figs. 14 and 15 for DNS and the model [Eq. (68)], respectively. [It may be recalled that (Sec. II A) in the model the kinetic energy $k$ is taken to be constant; with this assumption, model results for normalized correlation functions based on $\omega^*$ can be compared with DNS results based on $\epsilon$.] The correlation between $\omega^*$ and $\chi^*$ is important in determining the energy-dissipation-conditioned scalar statistics. Overall the shapes are similar: For negative $\tau$ [where $\rho(\tau)\propto\langle\omega^*(t)\chi^*(t+\tau)\rangle$] the functions decay more slower than for positive $\tau$. This suggests, in accordance with Eq. (23), that $\chi^*$ increases in response to increases in $\omega^*$. In other words, positive fluctuations in the energy dissipation rate lead (through the gradient amplification term) to positive fluctuations in the scalar dissipation rate.

## V. CONCLUSIONS AND DISCUSSION

Lagrangian time series from DNS over a range of Reynolds and Schmidt numbers have been used to validate La-

TABLE VI. Correlation coefficients for velocity ($u$) and scalars (1 and 2).

| | $\rho_{u1}$ | | | $\rho_{u2}$ | | | $\rho_{12}$ | | |
|---|---|---|---|---|---|---|---|---|---|
| $R_\lambda$ | DNS | LFP | LCN | DNS | LFP | LCN | DNS | LFP | LCN |
| 38 | −0.639 | −0.472 | −0.379 | −0.551 | −0.466 | −0.370 | 0.944 | 0.973 | 0.973 |
| 91 | −0.587 | −0.462 | −0.382 | −0.499 | −0.451 | −0.369 | 0.926 | 0.944 | 0.942 |
| 134 | −0.563 | −0.434 | −0.356 | −0.510 | −0.430 | −0.350 | 0.939 | 0.955 | 0.954 |
| 234 | −0.595 | −0.421 | −0.348 | −0.559 | −0.416 | −0.339 | 0.967 | 0.953 | 0.945 |

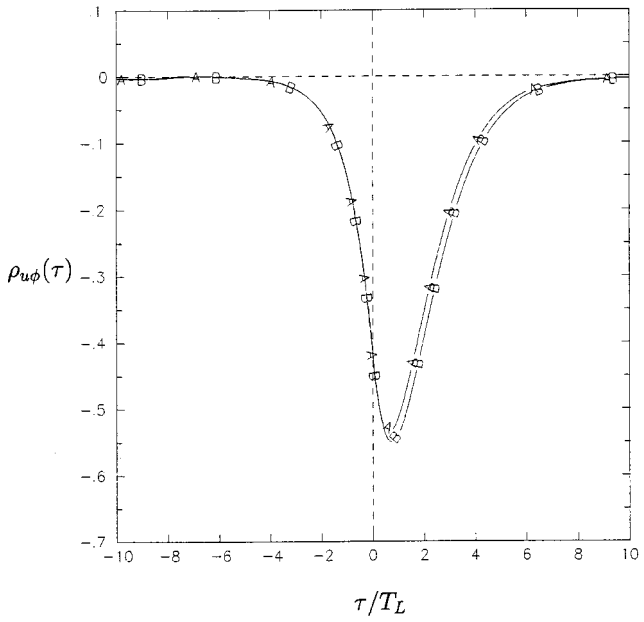


FIG. 12. Normalized Lagrangian velocity-scalar cross-correlation functions from the LFP model for the same conditions as in Fig. 11.

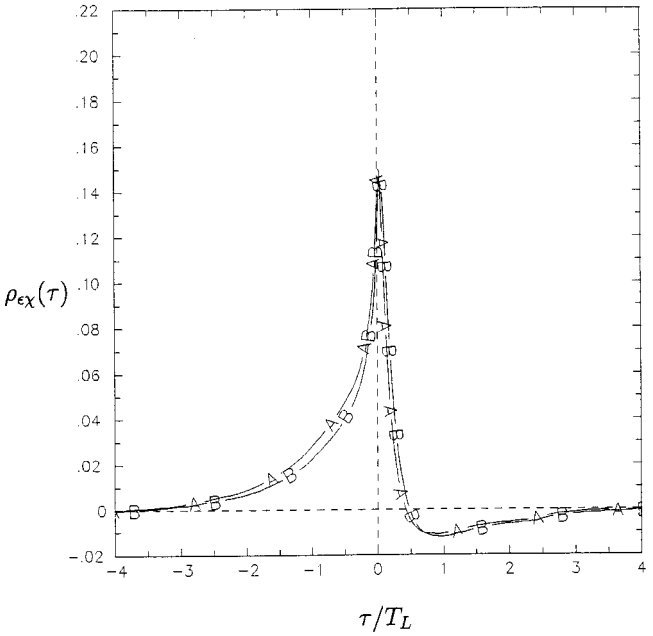


FIG. 14. Lagrangian cross-correlation functions between energy and scalar dissipation, from DNS for $R_\lambda$ 234. $\chi_1$ at $Sc=1/8$ (A). $\chi_2$ at $Sc=1$ (B). Note that the range of time lags shown is narrower than those in Figs. 11–13.

grangian stochastic models for scalar transport. In general, the agreement is satisfactory for both Eulerian and Lagrangian statistics in the quantities considered (i.e., velocity, energy dissipation, scalars, and scalar dissipation rates). Overall, the LCN model yields excellent agreement with the DNS scalar time series. Moreover, it is the only scalar mixing model currently available that reproduces Lagrangian scalar statistics accurately.

While we have demonstrated that the LCN model is successful at reproducing Lagrangian statistics, we also recognize that in other aspects the mixing models are still subject to certain deficiencies that remain to be addressed in future investigations. These are the following.

First, the parameter $C_1$ in the turbulence frequency model [Eq. (10)] affects both the integral time scale of $\omega^*$ and the conditional statistics $\langle\chi|\epsilon\rangle$ and $\langle\phi'^2|\epsilon\rangle$. Good agreement with DNS for the former requires $C_1$ to increase with Reynolds number, while for the latter $C_1$ should be independent of Reynolds number. From this observation, we can

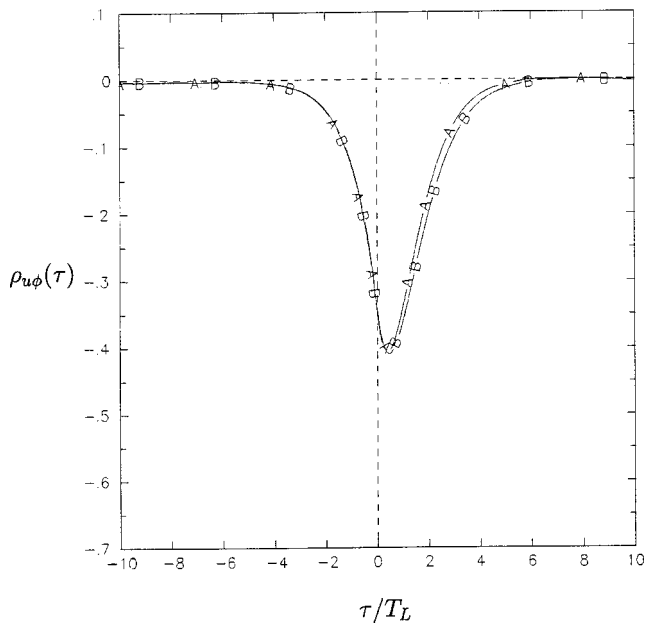


FIG. 13. Normalized Lagrangian velocity-scalar cross-correlation functions from the LCN model for the same conditions as in Fig. 11.

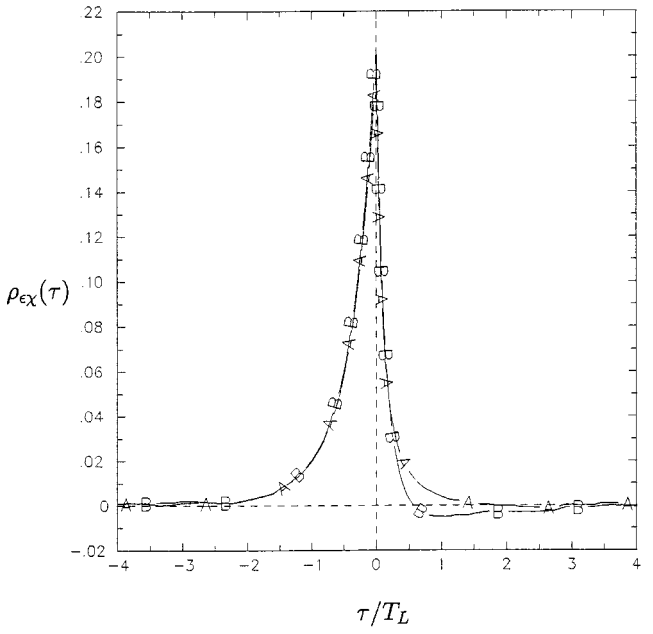


FIG. 15. Lagrangian cross-correlation functions between energy and scalar dissipation, from mixing model for the same conditions as in Fig. 14.

conclude that the time statistics of $\omega^*$ appearing in the gradient amplification term [Eq. (23)] must be different than those of $\epsilon^*$. Since the role of $\omega^*$ in the LSR model is to serve as the ''noise'' term in the scalar dissipation rate equation, it is appropriate to take $C_1$ to be independent of the Reynolds number. Likewise, to improve the agreement with the conditional statistics from DNS, $C_s$ appearing in Eq. (23) should, as in Fox,[4] be independent of $\omega^*$, and the value of the stretching exponent [Eq. (24)] should be $\gamma=1/2$.

Second, as seen in Figs. 5 and 6, Lagrangian statistics obtained from the LFP model do not produce a close match with DNS (particularly in the shape of the scalar autocorrelation functions). The LCN model provides better agreement by allowing the modeled scalar to be differentiable in time, but results for the velocity-scalar correlation are less accurate. Moreover, neither model correctly predicts the Reynolds-number dependence of the scalar difference (e.g., $\phi_1-\phi_2$). From these observations we conclude that a multiscale mixing model should be explored wherein the LFP model is used only in the scalar dissipation range. Such a model can be based on an extension of the LSR model to include random fluctuations in each wavenumber band. The variance of the scalar in a particular wavenumber band must be consistent with the LSR model. We plan to develop such a model in future work.

Third, the linear stochastic model for the fluctuating scalar dissipation rates $\chi^*_{\alpha\beta}(t)$ does not exhibit the same Reynolds and Schmidt-number dependence as observed in DNS. Better predictions will require a nonlinear model with PDF shape parameters that depend on $R_\lambda$ and $Sc$, in a manner similar to the way in which $R_\lambda$ dependence is incorporated into the model for $\omega^*$. However, since the LFP and LCN mixing models use only the conditional scalar dissipation rate $\langle\chi_{\alpha\beta}\rangle^*(t)$, such an extension is not essential at this time.

To conclude the paper, we consider here briefly how the mixing models presented in this work can be extended to non-Gaussian scalars such as those evolving from nonpremixed initial conditions. Different functional forms will be required for the scalar-conditioned joint scalar dissipation rates $\langle\boldsymbol{\chi}|\boldsymbol{\phi}\rangle^*$. For example, in the case of a mixture fraction variable $\xi$ restricted to the range $(0\leqslant\xi\leqslant1)$ evolving from nonpremixed initial conditions,[38] the form

$$\langle\chi|\xi=\zeta\rangle^*=\langle\chi\rangle^*\frac{\zeta(1-\zeta)}{\langle\xi(1-\xi)\rangle^*}, \tag{78}$$

yields a beta PDF for $\xi$. This result can be extended to multiple inert passive scalars[29] like those used in the DNS studies of Juneja and Pope[39] by using the surface-normal vector $\mathbf{n}_b(\boldsymbol{\phi}_b)$.

For example, the allowable region for the bivariate mixture fraction variables $\xi_1$ and $\xi_2$ is bounded by $0\leqslant\xi_1$, $0\leqslant\xi_2$ and $0\leqslant\xi_1+\xi_2\leqslant1$, and thus has three surface-normal vectors:

$$\mathbf{n}_b(0,\xi_2)=\begin{bmatrix}1\\0\end{bmatrix},\quad \mathbf{n}_b(\xi_1,0)=\begin{bmatrix}0\\1\end{bmatrix},\quad \mathbf{n}_b(\xi_1,1-\xi_1)=\begin{bmatrix}1\\1\end{bmatrix}. \tag{79}$$

By applying the constraint $\langle\boldsymbol{\chi}|\boldsymbol{\xi}=\boldsymbol{\zeta}_b\rangle^*\mathbf{n}_b(\boldsymbol{\zeta}_b)=0$ where $\boldsymbol{\zeta}_b$ is a point on the boundary, the conditional scalar dissipation rates can be modeled by[29]

$$\begin{aligned}\langle\chi_{11}|\zeta_1,\zeta_2\rangle^*&=C_{\chi1}\zeta_1(1-\zeta_1-\zeta_2)-C_{\chi2}\zeta_1\zeta_2,\\ \langle\chi_{12}|\zeta_1,\zeta_2\rangle^*&=C_{\chi2}\zeta_1\zeta_2,\\ \langle\chi_{22}|\zeta_1,\zeta_2\rangle^*&=C_{\chi3}\zeta_2(1-\zeta_1-\zeta_2)-C_{\chi2}\zeta_1\zeta_2,\end{aligned} \tag{80}$$

where the three constants $C_{\chi1}$, $C_{\chi2}$, and $C_{\chi3}$ are fixed by forcing $\langle\langle\boldsymbol{\chi}|\boldsymbol{\xi}\rangle^*\rangle^*=\langle\boldsymbol{\chi}\rangle^*$. [Note that Eq. (80) reduces to Eq. (78) for the univariate case.] Remarkably, due to the simple form of the surface-normal vectors, the definition of $\langle\boldsymbol{\chi}|\boldsymbol{\xi}\rangle^*$ for cases with three or more mixture-fraction variables follows from Eq. (80) by direct analogy.[29] Moreover, because the constants $C_{\chi\alpha}$ depend only on the means $(\langle\boldsymbol{\xi}\rangle^*)$ and the covariances $(\langle\boldsymbol{\xi}\boldsymbol{\xi}^{\mathrm{T}}\rangle^*)$, the resulting joint mixture-fraction PDF should correspond to a multivariate beta PDF.

By making a linear change of variables

$$\boldsymbol{\phi}=\frac{1}{2}\begin{bmatrix}-\sqrt{3}&\sqrt{3}\\-3&-3\end{bmatrix}\boldsymbol{\xi}+\begin{bmatrix}0\\1\end{bmatrix}, \tag{81}$$

Eq. (80) can be used to treat the equal-diffusivity, two-scalar mixing cases in Juneja and Pope[39] (i.e., the so-called three-stream mixing problem). Examples of the joint PDF predicted using the LFP model are shown in Fig. 16 for several values of the standardized scalar variance. For this case, the time scales $(r_\phi)$ for both scalars are taken to be identical. The agreement with the corresponding DNS data of Juneja and Pope[39] is excellent. Effects of initial scalar integral scale and differential-diffusion[39] can be treated by using the simple spectral description for $\langle\boldsymbol{\chi}\rangle^*$ provided by the LSR model.[3,4] The Lagrangian mixing models presented in this work are the only ones capable of modeling such effects for multivariate (i.e., three or more streams) mixing problems.

For multiple reacting scalars, the modeling challenges are much greater due to the interactions between the chemistry and the scalar dissipation rate. Thus, DNS data like those used in this work will be crucial for model formulation and validation. Note that, in principle, chemical reactions should affect both the scalar time scales (i.e., $\langle\boldsymbol{\chi}\rangle^*$) and the shape of the joint scalar PDF. In the multivariate case, the latter is determined by the scalar-dependent ''PDF-shape'' matrix[29]

$$\mathbf{H}(\boldsymbol{\phi})\equiv\mathbf{S}_\chi^{-1}\langle\boldsymbol{\chi}|\boldsymbol{\phi}\rangle^*\mathbf{S}_\chi^{-1}. \tag{82}$$

Only very recently have data on $\mathbf{H}(\boldsymbol{\phi})$ been extracted from DNS,[40] for a single-step reaction. Note that for the Gaussian scalars used in this work $\mathbf{H}(\boldsymbol{\phi})=\mathbf{g}^\dagger$, where $\mathbf{g}^\dagger$ is the energy-dissipation-conditioned gradient correlation matrix [Eq. (35)]. More generally, $\mathbf{H}(\boldsymbol{\phi})$ will often be rank deficient (i.e., some of the scalars being linearly dependent) and have a nontrivial dependence on $\boldsymbol{\phi}$. Moreover, with differential diffusion the rank of $\mathbf{H}(\boldsymbol{\phi})$ may change as mixing proceeds. Similar effects can also be expected from chemical reactions [e.g., instantaneous reactions will lead to algebraic constraints[29] on sets of scalars and thereby lower the rank of

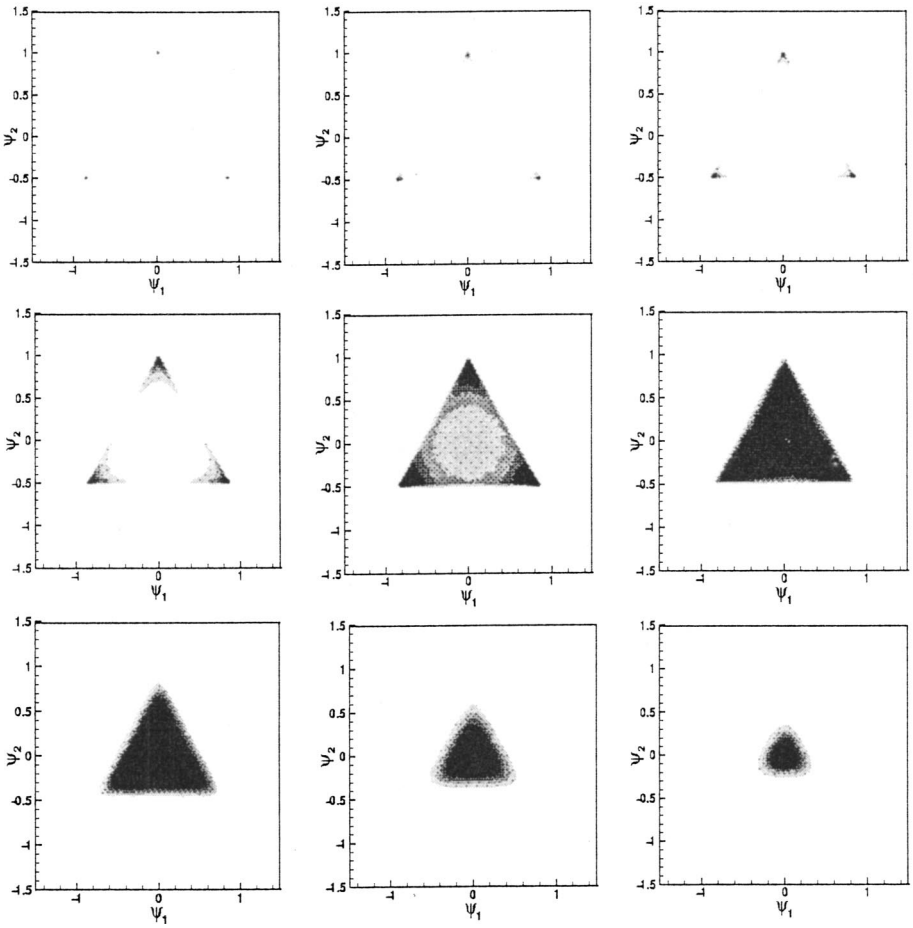

FIG. 16. Bivariate scalar PDF for three-stream mixing predicted by the LFP model. From left-to-right, top-to-bottom: $\Phi \equiv (\langle \phi'^2(t)\rangle / \langle \phi'^2(0)\rangle)^{1/2} = 1.0$, 0.9, 0.8, 0.7, 0.6, 0.5, 0.4, 0.3, and 0.2.

$\mathbf{H}(\boldsymbol{\phi})$]. Thus, due to its critical role in scalar mixing models, further investigations into the behavior and modeling of $\mathbf{H}(\boldsymbol{\phi})$ would be of particular interest.

## ACKNOWLEDGMENTS

The authors gratefully acknowledge support by the National Science Foundation via Grant Nos. CTS-9705678 (PKY) and CTS-9985678 (ROF). Additional partial support was provided by NSF cooperative agreement ACI-9619020 through computing resources provided by the National Partnership for Advanced Computational Infrastructure at the San Diego Supercomputer Center. We also thank V. Raman for generating the simulation data used to produce Fig. 16.

## APPENDIX: DERIVATION OF CORRELATION FUNCTIONS

As seen in the comparisons made in this paper, some of the most important output statistics of a Lagrangian stochastic model are the correlation functions. It is thus of great interest to understand the effects of model parameters on the correlation functions. Analytical derivations of the correlation functions are possible[30] for linear stochastic differential equations (SDE) with constant coefficients. Although (due to the time dependence of $\boldsymbol{\chi}^*$) the SDE's used in this work have variable coefficients, we can still obtain useful insights as shown below by assuming constant coefficients.

The general form for a multivariate Ornstein–Uhlenbeck process is

$$\mathrm{d}\mathbf{x}(t) = -\mathbf{A}\mathbf{x}(t)\mathrm{d}t + \mathbf{B}\mathrm{d}\mathbf{W}(t), \tag{A1}$$

where $\mathbf{x}$ is a vector of state variables (e.g., $[u^*, \phi_1'^*, \phi_2'^*]^{\mathrm{T}}$) of $N$ elements, and $\mathbf{A}$ and $\mathbf{B}$ are constant matrices whose exact form depends on the model (e.g., LFP or LCN). The state variables will attain a statistically stationary state provided that the matrix $\mathbf{A}$ is positive definite (which will usually be the case). The linear SDE then admits an integral solution of the form

$$\mathbf{x}(t) = \int_{-\infty}^{t} \exp[-\mathbf{A}(t-t')]\mathbf{B}\mathrm{d}\mathbf{W}(t'). \tag{A2}$$

Using the Wiener process property $\langle \mathrm{d}\mathbf{W}(t)\mathrm{d}\mathbf{W}^{\mathrm{T}}(s)\rangle = \mathbf{I}\delta(t-s)$ [where $\delta(\cdot)$ is the Dirac delta function], the resulting unnormalized correlation-function matrix can be written as

$$\langle \mathbf{x}(t)\mathbf{x}^{\mathrm{T}}(s)\rangle = \int_{-\infty}^{\min(t,s)} \exp[-\mathbf{A}(t-t')]\mathbf{B}\mathbf{B}^{\mathrm{T}} \times \exp[-\mathbf{A}^{\mathrm{T}}(s-t')]\mathrm{d}t'. \tag{A3}$$

For a stationary process this integral depends only on the time difference $\tau \equiv t-s$.

The integral in Eq. (A3) can be evaluated analytically if both $\mathbf{A}$ and $\mathbf{B}$ are constants. Defining the covariance matrix by

$$\boldsymbol{\sigma}^2 \equiv \langle \mathbf{x}(t)\mathbf{x}^{\mathrm{T}}(t)\rangle, \tag{A4}$$

a linear algebraic equation results from Eq. (A3) (see Gardiner[30] for details)

$$\mathbf{A}\boldsymbol{\sigma}^2 + \boldsymbol{\sigma}^2\mathbf{A}^{\mathrm{T}} = \mathbf{B}\mathbf{B}^{\mathrm{T}}. \tag{A5}$$

Note that because both sides of this equation represent symmetric $N\times N$ matrices, the $N(N+1)/2$ independent components can be rewritten and solved as a linear system for the unknown elements of $\boldsymbol{\sigma}^2$.

Given the covariance matrix, the unnormalized correlation-function matrix can be evaluated by rearranging Eq. (A3) and using Eq. (A5) (see Gardiner[30] for details). Furthermore, the result can be normalized by defining a diagonal matrix using the standard deviations $\mathbf{S}_x \equiv \mathbf{diag}(\langle x_1^2\rangle^{1/2},\ldots,\langle x_N^2\rangle^{1/2})$. The correlation-function matrix is then given by

$$\begin{aligned}\boldsymbol{\rho}_x(\tau) &\equiv \mathbf{S}_x^{-1}\langle \mathbf{x}(t)\mathbf{x}^{\mathrm{T}}(s)\rangle \mathbf{S}_x^{-1} \\ &= \begin{cases} \mathbf{S}_x^{-1}\exp(-\mathbf{A}|\tau|)\mathbf{S}_x\boldsymbol{\rho}_x & \text{if } \tau>0, \\ \boldsymbol{\rho}_x\mathbf{S}_x\exp(-\mathbf{A}^{\mathrm{T}}|\tau|)\mathbf{S}_x^{-1} & \text{if } \tau<0, \end{cases}\end{aligned} \tag{A6}$$

where the correlation matrix is $\boldsymbol{\rho}_x \equiv \mathbf{S}_x^{-1}\boldsymbol{\sigma}^2\mathbf{S}_x^{-1}$. Note that the $\tau$-dependence of $\boldsymbol{\rho}_x(\tau)$ is expressed only via the drift matrix $\mathbf{A}$, and not the diffusion matrix $\mathbf{B}$. On the other hand, $\mathbf{B}$ will affect the correlation matrix through Eq. (A5).

The correlation time matrix can be defined by

$$\mathbf{T}_x \equiv \int_0^\infty \boldsymbol{\rho}_x(\tau)\,\mathrm{d}\tau = \mathbf{S}_x^{-1}\mathbf{A}^{-1}\mathbf{S}_x\boldsymbol{\rho}_x. \tag{A7}$$

The diagonal elements of $\mathbf{T}_x$ are the Lagrangian autocorrelation times. Given the general theory, we will now look at specific applications of Eqs. (A5)–(A7) to the LFP and LCN models.

### 1. LFP model

For the LFP model, the state vector can be defined as $\mathbf{x} = [u^*, v_1^*, v_2^*]^{\mathrm{T}}$ where $v_\alpha^* \equiv \phi_\alpha'^*/\langle \phi_\alpha'^2\rangle^{1/2}$ are the standardized scalars. The constant-coefficient SDE has the form of Eq. (7) combined with

$$\begin{aligned}\mathrm{d}\mathbf{v}^* = &-G\mathbf{S}_\phi^{-1}\mathbf{1}u^*\mathrm{d}t - \tfrac{1}{2}[\mathbf{S}_D\mathbf{r}_\phi\mathbf{S}_D^{-1} + C_2\mathbf{r}_\phi]\boldsymbol{\rho}_\phi^{-1}\mathbf{v}^*\mathrm{d}t \\ &+ (C_2\mathbf{r}_\phi)^{1/2}\mathrm{d}\mathbf{W},\end{aligned} \tag{A8}$$

where $\mathbf{r}_\phi \equiv \mathbf{S}_\phi^{-1}\boldsymbol{\chi}\mathbf{S}_\phi^{-1}$ and $\boldsymbol{\rho}_\phi \equiv \langle \mathbf{v}\mathbf{v}^{\mathrm{T}}\rangle$ is the scalar correlation matrix.

The coefficient matrices from the LFP model have the form

$$\mathbf{B}\mathbf{B}^{\mathrm{T}} = \begin{bmatrix} b_{11} & 0 & 0 \\ 0 & b_{22} & b_{23} \\ 0 & b_{32} & b_{33} \end{bmatrix}, \tag{A9}$$

where $b_{11} = 3C_0/2$

$$\begin{bmatrix} b_{22} & b_{23} \\ b_{32} & b_{33} \end{bmatrix} = C_2\mathbf{r}_\phi \tag{A10}$$

and

$$\mathbf{A} = \begin{bmatrix} a_{11} & 0 & 0 \\ a_{21} & a_{22} & a_{23} \\ a_{31} & a_{32} & a_{33} \end{bmatrix}, \tag{A11}$$

where $a_{11} = 3C_0/4$, $a_{21} = G/\langle \phi_1'^2\rangle^{1/2}$, $a_{31} = G/\langle \phi_2'^2\rangle^{1/2}$, and

$$\begin{bmatrix} a_{22} & a_{23} \\ a_{32} & a_{33} \end{bmatrix} = \frac{1}{2}[\mathbf{S}_D\mathbf{r}_\phi\mathbf{S}_D^{-1} + C_2\mathbf{r}_\phi]\boldsymbol{\rho}_\phi^{-1}. \tag{A12}$$

Because the variables are normalized, the covariance matrix is given by

$$\boldsymbol{\sigma}^2 = \begin{bmatrix} 1 & \rho_{u1} & \rho_{u2} \\ \rho_{u1} & 1 & \rho_{12} \\ \rho_{u2} & \rho_{12} & 1 \end{bmatrix}. \tag{A13}$$

From this expression, Eq. (A5) might appear to be overdetermined since it provides six independent equations for three unknowns (i.e., $\rho_{u1}$, $\rho_{u2}$, and $\rho_{12}$). However, $\langle \phi_1'^2\rangle$ and $\langle \phi_2'^2\rangle$ are also unknown and must be determined from two of the diagonal elements of Eq. (A5). The third diagonal element leads to a trivial identity as shown below [Eq. (A17)].

With the matrix $\mathbf{A}$ given as in Eq. (A11), the correlation time matrix can now be found from Eq. (A7). Furthermore, At this point, the matrix exponentials appearing in Eq. (A6) can be determined analytically using the eigenvectors and eigenvalues of $\mathbf{A}$

$$\exp(\mathbf{A}|\tau|) = \boldsymbol{\Psi}\exp(\boldsymbol{\Lambda}|\tau|)\boldsymbol{\Psi}^{-1}, \tag{A14}$$

where $\boldsymbol{\Psi}$ is the matrix of eigenvectors and $\boldsymbol{\Lambda}$ is the corresponding eigenvalue matrix. If the eigenvalues are unique, then $\boldsymbol{\Lambda} = \mathbf{diag}(\lambda_1,\ldots,\lambda_N)$ and $\exp(\boldsymbol{\Lambda}|\tau|) = \mathbf{diag}(e^{\lambda_1|\tau|},\ldots,e^{\lambda_N|\tau|})$. For the two-scalar case, the results are rather complicated and unenlightening. Thus, we will continue the analysis for the single-scalar case where the two eigenvalues of $\mathbf{A}$ are given by $\lambda_1 = a_{11}$ and $\lambda_2 = a_{22}$.

After computing the eigenvectors needed in Eq. (A14), the correlation functions reduce to Eq. (8)

$$\rho_{u\phi}(\tau) = \begin{cases} \rho_{u\phi}e^{a_{11}\tau} & \text{if } \tau<0 \\ \rho_{u\phi}e^{-a_{22}\tau} + \dfrac{a_{21}}{a_{11}-a_{22}}(e^{-a_{11}\tau} - e^{-a_{22}\tau}) & \text{if } \tau>0 \end{cases} \tag{A15}$$

and

$$\rho_\phi(\tau) = e^{-a_{22}|\tau|} + \frac{\rho_{u\phi}a_{21}}{a_{11}-a_{22}}(e^{-a_{11}|\tau|} - e^{-a_{22}|\tau|}), \tag{A16}$$

where $a_{22} = (1+C_2)r_\phi/2$. Likewise, Eq. (A5) reduces to three equations

$$2a_{11} = b_{11}, \tag{A17}$$

$$2a_{21}\rho_{u\phi} + 2a_{22} = b_{22}, \tag{A18}$$

and

$$(a_{11}+a_{22})\rho_{u\phi} + a_{21} = 0, \tag{A19}$$

where $b_{22}=C_2 r_\phi$. Given the definitions of $a_{11}$ and $b_{11}$, the first equation is trivial. Inserting the definitions of the remaining coefficients, the second and third equations yield

$$\langle \phi'^2 \rangle = \frac{2G^2}{r_\phi[\frac{3}{4}C_0 + \frac{1}{2}(1+C_2)r_\phi]} \tag{A20}$$

and

$$\rho_{u\phi} = -\left[\frac{r_\phi}{\frac{3}{2}C_0 + (1+C_2)r_\phi}\right]^{1/2}. \tag{A21}$$

Note that, as stated in the main text, $C_2$ controls the decay rate of $\rho_\phi(\tau)$. Integrating Eq. (A16) to find the Lagrangian scalar integral scale yields

$$T_\phi = \frac{2}{(1+C_2)r_\phi} + \frac{4}{3(1+C_2)C_0}, \tag{A22}$$

from which the influence of $C_2$ is clearly evident. In addition

$$\left.\frac{\mathrm{d}\rho_\phi}{\mathrm{d}\tau}\right|_{\tau=0} = -a_{22} - \rho_{u\phi}a_{21} = -\frac{1}{2}C_2 r_\phi, \tag{A23}$$

so that $C_2$ also controls the slope of the scalar autocorrelation function at the origin.

### 2. LCN model

For the two-scalar LCN model, the state vector has five components, i.e., $\mathbf{x}=[u^*, h_1^*, h_2^*, v_1^*, v_2^*]^{\mathrm{T}}$. The constant-coefficient SDE has the form of Eq. (7) combined with

$$\mathrm{d}\mathbf{h}^* = -\frac{C_3}{2}\mathbf{S}_\tau^{-1}\mathbf{h}^*\mathrm{d}t + (C_3\mathbf{S}_\tau^{-1})^{1/2}\mathrm{d}\mathbf{W} \tag{A24}$$

and

$$\mathrm{d}\mathbf{v}^* = -G\mathbf{S}_\phi^{-1}\mathbf{1}u^*\mathrm{d}t + \tfrac{1}{2}C_2\mathbf{r}_\phi\mathbf{h}^*\mathrm{d}t - \tfrac{1}{2}[\mathbf{S}_D\mathbf{r}_\phi\mathbf{S}_D^{-1} + C_2\mathbf{S}_\tau^{-1}\mathbf{D}\mathbf{S}_\tau^{-1}]\boldsymbol{\rho}_\phi^{-1}\mathbf{v}^*\mathrm{d}t, \tag{A25}$$

where $\mathbf{S}_\tau = \mathbf{diag}(\tau_1, \tau_2)$ is the scalar time scale matrix and $\mathbf{D}$ has the form of Eq. (59).

The coefficient matrices from the LCN model have the form

$$\mathbf{B}\mathbf{B}^{\mathrm{T}} = \begin{bmatrix} b_{11} & 0 & 0 & 0 & 0 \\ 0 & b_{22} & 0 & 0 & 0 \\ 0 & 0 & b_{33} & 0 & 0 \\ 0 & 0 & 0 & 0 & 0 \\ 0 & 0 & 0 & 0 & 0 \end{bmatrix}, \tag{A26}$$

where $b_{11}=3C_0/2$, $b_{22}=C_3/\tau_1$, and $b_{33}=C_3/\tau_2$; and

$$\mathbf{A} = \begin{bmatrix} a_{11} & 0 & 0 & 0 & 0 \\ 0 & a_{22} & 0 & 0 & 0 \\ 0 & 0 & a_{33} & 0 & 0 \\ a_{41} & a_{42} & a_{43} & a_{44} & a_{45} \\ a_{51} & a_{52} & a_{53} & a_{54} & a_{55} \end{bmatrix}, \tag{A27}$$

where $a_{11}=3C_0/4$, $a_{22}=C_3/(2\tau_1)$, $a_{33}=C_3/(2\tau_2)$, $a_{41}=G/\langle \phi_1'^2 \rangle^{1/2}$, $a_{51}=G/\langle \phi_2'^2 \rangle^{1/2}$,

$$\begin{bmatrix} a_{42} & a_{43} \\ a_{52} & a_{53} \end{bmatrix} = -\frac{1}{2}C_2\mathbf{r}_\phi \tag{A28}$$

and

$$\begin{bmatrix} a_{44} & a_{45} \\ a_{54} & a_{55} \end{bmatrix} = \frac{1}{2}[\mathbf{S}_D\mathbf{r}_\phi\mathbf{S}_D^{-1} + C_2\mathbf{S}_\tau^{-1}\mathbf{D}\mathbf{S}_\tau^{-1}]\boldsymbol{\rho}_\phi^{-1}. \tag{A29}$$

Because the variables are normalized, the covariance matrix is given by

$$\boldsymbol{\sigma}^2 = \begin{bmatrix} 1 & 0 & 0 & \rho_{u1} & \rho_{u2} \\ 0 & 1 & 0 & \langle h_1 v_1 \rangle & \langle h_1 v_2 \rangle \\ 0 & 0 & 1 & \langle h_2 v_1 \rangle & \langle h_2 v_2 \rangle \\ \rho_{u1} & \langle h_1 v_1 \rangle & \langle h_2 v_1 \rangle & 1 & \rho_{12} \\ \rho_{u2} & \langle h_1 v_2 \rangle & \langle h_2 v_2 \rangle & \rho_{12} & 1 \end{bmatrix}. \tag{A30}$$

The one-scalar case is obtained by removing the third and fifth rows and columns from Eqs. (A26), (A27), and (A30). The eigenvalues of the resulting $\mathbf{A}$ matrix are given by $a_{11}$, $a_{22}$, and $a_{44}$. After finding the corresponding eigenvectors, the correlation functions reduce to Eq. (8),

$$\rho_h(\tau) = e^{-a_{22}|\tau|}, \tag{A31}$$

$$\rho_{u\phi}(\tau) = \begin{cases} \rho_{u\phi}e^{a_{11}\tau} & \text{if } \tau<0 \\ \rho_{u\phi}e^{-a_{44}\tau} + \dfrac{a_{41}}{a_{11}-a_{44}}(e^{-a_{11}\tau} - e^{-a_{44}\tau}) & \text{if } \tau>0 \end{cases}, \tag{A32}$$

$$\rho_{h\phi}(\tau) = \begin{cases} \langle hv \rangle e^{a_{22}\tau} & \text{if } \tau<0 \\ \langle hv \rangle e^{-a_{44}\tau} + \dfrac{a_{42}}{a_{22}-a_{44}}(e^{-a_{22}\tau} - e^{-a_{44}\tau}) & \text{if } \tau>0 \end{cases}, \tag{A33}$$

and

$$\rho_\phi(\tau) = e^{-a_{44}|\tau|} + \frac{\rho_{u\phi}a_{41}}{a_{11}-a_{44}}(e^{-a_{11}|\tau|} - e^{-a_{44}|\tau|}) + \frac{\langle hv \rangle a_{42}}{a_{22}-a_{44}}(e^{-a_{22}|\tau|} - e^{-a_{44}|\tau|}), \tag{A34}$$

where $a_{44}=(1+C_2\langle hv \rangle)r_\phi/2$. Likewise, Eq. (A5) reduces to three nontrivial equations

$$(a_{11}+a_{44})\rho_{u\phi} + a_{41} = 0, \tag{A35}$$

$$(a_{22}+a_{44})\langle hv \rangle + a_{42} = 0, \tag{A36}$$

$$a_{41}\rho_{u\phi} + a_{42}\langle hv \rangle + a_{44} = 0, \tag{A37}$$

where $a_{41}=G/\langle \phi'^2 \rangle^{1/2}$ introduces the third unknown. Using Eq. (61), we can write $C_2\langle hv \rangle = 2$ so that $a_{44}=3r_\phi/2$. The three equations can then be manipulated to obtain the results

$$\langle hv \rangle = \left(\frac{2}{3+C_3}\right)^{1/2}, \tag{A38}$$

$$\langle \phi'^2 \rangle = \frac{2G^2}{r_\phi(\frac{3}{4}C_0 + \frac{3}{2}r_\phi)}, \tag{A39}$$

$$\rho_{u\phi} = -\left( \frac{r_\phi}{\frac{3}{2}C_0 + 3r_\phi} \right)^{1/2}. \tag{A40}$$

Comparing with the LFP model, setting $C_2 = 2$ in Eqs. (A20) and (A21) yields the same values for $\langle \phi'^2 \rangle$ and $\rho_{u\phi}$ as the LCN model.

Note that, as stated in the main text, $C_3$ can be used to control the decay rate of $\rho_\phi(\tau)$ by varying $a_{22}$ in Eq. (A34). Integration of Eq. (A34) gives the scalar integral time scale as

$$T_\phi = \frac{2}{3r_\phi} + \frac{4}{9C_0} + \frac{4}{3C_3 r_\phi}. \tag{A41}$$

This expression reduces to Eq. (A22) (with $C_2 = 2$) in the limit where $C_3$ goes to infinity. In addition

$$\left. \frac{\mathrm{d}\rho_\phi}{\mathrm{d}\tau} \right|_{\tau=0} = -a_{44} - \rho_{u\phi}a_{41} - \langle hv \rangle a_{42} = 0, \tag{A42}$$

so that the scalar autocorrelation function has the correct slope of zero at the origin.


[1] S. B. Pope, "PDF methods for turbulent reactive flows," Prog. Energy Combust. Sci. **11**, 119 (1985).
[2] S. B. Pope, "Lagrangian pdf methods for turbulent flows," Annu. Rev. Fluid Mech. **26**, 23 (1994).
[3] R. O. Fox, "The Lagrangian spectral relaxation model of the scalar dissipation in homogeneous turbulence," Phys. Fluids **9**, 2364 (1997).
[4] R. O. Fox, "The Lagrangian spectral relaxation model for differential diffusion in homogeneous turbulence," Phys. Fluids **11**, 1550 (1999).
[5] P. K. Yeung, "Correlations and conditional statistics in differential diffusion: Scalars with mean scalar gradients," Phys. Fluids **10**, 2621 (1998).
[6] S. B. Pope, *Turbulent Flows* (Cambridge University Press, Cambridge, 2000).
[7] G. A. Voth, K. Satyanarayanan, and E. Bodenschatz, "Lagrangian acceleration measurements at large Reynolds numbers," Phys. Fluids **10**, 2268 (1998).
[8] S. Ott and J. Mann, "An experimental investigation of the relative diffusion of particle pairs in three-dimensional turbulent flow," J. Fluid Mech. **422**, 207 (2000).
[9] N. Mordant, P. Metz, O. Michel, and J. F. Pinton, "Measurement of Lagrangian velocity in fully developed turbulence," Phys. Rev. Lett. **87**, 214501 (2001).
[10] P. K. Yeung, "Lagrangian characteristics of turbulence and scalar transport in direct numerical simulations," J. Fluid Mech. **427**, 241 (2001).
[11] B. L. Sawford and P. K. Yeung, "Eulerian acceleration statistics as a discriminator between Lagrangian stochastic models in uniform shear flow," Phys. Fluids **12**, 2033 (2000).
[12] B. L. Sawford and P. K. Yeung, "Lagrangian statistics in uniform shear flow: Direct numerical simulation and Lagrangian stochastic models," Phys. Fluids **13**, 2627 (2001).
[13] P. Vedula, P. K. Yeung, and R. O. Fox, "Dynamics of scalar dissipation in isotropic turbulence: A numerical and modeling study," J. Fluid Mech. **433**, 29 (2001).
[14] J. Villermaux and J. C. Devillon, "Représentation de la coalescence et de la redispersion des domaines de ségrégation dans un fluide par un modèle d'interaction phénoménologique," *Proc., 2nd International Symposium on Chemical Reaction Engineering* (Elsevier, New York, 1972).
[15] L. Valiño and C. Dopazo, "A binomial Langevin model for turbulent mixing," Phys. Fluids A **3**, 3034 (1991).
[16] S. Subramaniam and S. B. Pope, "A mixing model for turbulent reactive flows based on Euclidean minimum spanning trees," Combust. Flame **115**, 487 (1998).
[17] H. Chen, S. Chen, and R. S. Kraichnan, "Probability distribution of a stochastically advected scalar field," Phys. Rev. Lett. **63**, 2657 (1989).
[18] B. L. Sawford, private communication (2001).
[19] P. K. Yeung, "Lagrangian investigations of turbulence," Annu. Rev. Fluid Mech. **34**, 115 (2002).
[20] R-C. Lien and E. A. D'Asaro, "The Kolmogorov constant for the Lagrangian velocity spectrum and structure function," Phys. Fluids **14**, 4456 (2002).
[21] M. R. Overholt and S. B. Pope, "Direct numerical simulation of a passive scalar with imposed mean gradient in isotropic turbulence," Phys. Fluids **8**, 3128 (1996).
[22] P. K. Yeung and S. B. Pope, "Lagrangian statistics from direct numerical simulations of isotropic turbulence," J. Fluid Mech. **207**, 531 (1989).
[23] R. O. Fox, "On velocity-conditioned scalar mixing in homogeneous turbulence," Phys. Fluids **8**, 2678 (1996).
[24] R. O. Fox and P. K. Yeung, "Forward and backward spectral transfer in the modeling of scalar mixing in homogeneous turbulence," Proc., 3rd ASME/JSME Joint Fluids Engineering Conference, San Francisco, CA, July 1999.
[25] P. Vedula, "Study of scalar transport in turbulent flows using direct numerical simulations," Ph.D. thesis, School of Aerospace Engineering, Georgia Institute of Technology, Atlanta, GA (2001).
[26] J. P. H. Sanders and I. Gökalp, "Scalar dissipation rate modeling in variable density turbulent axisymmetric jets and diffusion flames," Phys. Fluids **10**, 938 (1998).
[27] R. O. Fox, "The spectral relaxation model of the scalar dissipation rate in homogeneous turbulence," Phys. Fluids **7**, 1082 (1995).
[28] C. M. Cha, G. Kosály, and H. Pitsch, "Modeling extinction and reignition in turbulent nonpremixed combustion using a doubly conditional moment closure approach," Phys. Fluids **13**, 3824 (2001).
[29] R. O. Fox, *Computational Models for Turbulent Reacting Flows* (Cambridge University Press, Cambridge, 2003).
[30] C. W. Gardiner, *Handbook of Stochastic Methods*, 2nd ed. (Springer, New York, 1990).
[31] R. O. Fox, "Improved Fokker–Planck model for the joint scalar, scalar gradient PDF," Phys. Fluids **6**, 334 (1994).
[32] A. Kerstein, "A linear-eddy model of turbulent scalar transport and mixing," Combust. Sci. Technol. **60**, 391 (1998).
[33] A. Kerstein, "One-dimensional turbulence model," J. Fluid Mech. **392**, 277 (1999).
[34] T. Dreeben and S. B. Pope, "Wall-function treatment in PDF methods for turbulent flows," Phys. Fluids **9**, 2692 (1997).
[35] P. K. Yeung and B. L. Sawford, "Random sweeping hypothesis for passive scalars in isotropic turbulence," J. Fluid Mech. **459**, 129 (2002).
[36] B. L. Sawford, "Reynolds number effects in Lagrangian stochastic models of turbulent dispersion," Phys. Fluids A **3**, 1577 (1991).
[37] S. B. Pope, "A stochastic Lagrangian model for acceleration in turbulent flows," Phys. Fluids **14**, 2447 (2002).
[38] R. O. Fox, P. K. Yeung, and P. Vedula, "Lagrangian description of nonpremixed passive scalars in differential diffusion: Model development," Bull. Am. Phys. Soc. **45**, 58 (2000).
[39] A. Juneja and S. B. Pope, "A DNS study of turbulent mixing of two passive scalars," Phys. Fluids **8**, 2161 (1996).
[40] C. M. Cha, P. Trouillet, and R. O. Fox, "Lagrangian PDF mixing models for reacting flows," Proceedings of the 2002 CTR Summer Program, Stanford, CA, July–August 2002.